

JGR Atmospheres

RESEARCH ARTICLE

10.1029/2018JD028955

Key Points:

- Oil and gas development is the largest source of ethane and propane in the United States; this sector is the third largest source of C₄-C₅ alkanes
- Propane is underpredicted over several U.S. regions
- Boundary layer enhancements of C₂-C₅ alkanes mixing ratios are largest over the central United States

Correspondence to:

E. V. Fischer,
evf@atmos.colostate.edu

Citation:

Tzompa-Sosa, Z. A., Henderson, B. H., Keller, C. A., Travis, K., Mahieu, E., Franco, B., et al. (2019). Atmospheric implications of large C₂-C₅ alkane emissions from the U.S. oil and gas industry. *Journal of Geophysical Research: Atmospheres*, 124, 1148–1169. <https://doi.org/10.1029/2018JD028955>

Received 7 MAY 2018

Accepted 18 DEC 2018

Accepted article online 22 DEC 2018

Published online 25 JAN 2019

Author Contributions:

Conceptualization: Z. A. Tzompa-Sosa, K. Travis, S. Conway, E. V. Fischer

Data curation: Z. A. Tzompa-Sosa, C. A. Keller, E. Mahieu, M. Estes, D. Helmig, E. V. Fischer

Formal analysis: Z. A. Tzompa-Sosa, S. Conway

Funding acquisition: Z. A. Tzompa-Sosa, E. V. Fischer

Investigation: Z. A. Tzompa-Sosa, E. V. Fischer

Methodology: Z. A. Tzompa-Sosa, C. A. Keller, K. Travis, S. Conway, E. V. Fischer

Resources: E. V. Fischer
















Supervision: E. V. Fischer

Writing - original draft: Z. A. Tzompa-Sosa, E. V. Fischer

Writing - review & editing: Z. A. Tzompa-Sosa, B. H. Henderson, C. A. Keller, K. Travis, E. Mahieu, B. Franco, D. Helmig, A. Fried, D. Richter, P. Weibring, J. Walega, D. R. Blake, J. W. Hannigan, I. Ortega, S. Conway, K. Strong, E. V. Fischer

©2018. American Geophysical Union.
All Rights Reserved.

Atmospheric Implications of Large C₂-C₅ Alkane Emissions From the U.S. Oil and Gas Industry

Z. A. Tzompa-Sosa¹ , B. H. Henderson² , C. A. Keller^{3,4} , K. Travis⁵ , E. Mahieu⁶ , B. Franco⁷ , M. Estes⁸, D. Helmig⁹ , A. Fried⁹ , D. Richter⁹ , P. Weibring⁹, J. Walega⁹, D. R. Blake¹⁰ , J. W. Hannigan¹¹ , I. Ortega¹¹ , S. Conway¹² , K. Strong¹² , and E. V. Fischer¹ 

¹Department of Atmospheric Science, Colorado State University, Fort Collins, CO, USA, ²Air Quality Modeling Group, Office of Air Quality Planning and Standards, U.S. Environmental Protection Agency, Washington, DC, USA,

³Universities Space Research Association/GESTAR, Columbia, MD, USA, ⁴Global Modeling and Assimilation Office, NASA Goddard Space Flight Center, Greenbelt, MD, USA, ⁵Department of Civil and Environmental Engineering, Massachusetts Institute of Technology, Cambridge, MA, USA, ⁶Institut d'Astrophysique et de Géophysique, Université de Liège, Liège, Belgium, ⁷Université libre de Bruxelles (ULB), Atmospheric Spectroscopy, Service de Chimie Quantique et Photophysique, Brussels, Belgium, ⁸Texas Commission on Environmental Quality, Austin, TX, USA, ⁹Institute of Arctic and Alpine Research, University of Colorado Boulder, Boulder, CO, USA, ¹⁰Department of Chemistry, University of California, Irvine, CA, USA, ¹¹National Center for Atmospheric Research, Boulder, CO, USA, ¹²Department of Physics, University of Toronto, Toronto, Ontario, Canada

Abstract Emissions of C₂-C₅ alkanes from the U.S. oil and gas sector have changed rapidly over the last decade. We use a nested GEOS-Chem simulation driven by updated 2011NEI emissions with aircraft, surface, and column observations to (1) examine spatial patterns in the emissions and observed atmospheric abundances of C₂-C₅ alkanes over the United States and (2) estimate the contribution of emissions from the U.S. oil and gas industry to these patterns. The oil and gas sector in the updated 2011NEI contributes over 80% of the total U.S. emissions of ethane (C₂H₆) and propane (C₃H₈), and emissions of these species are largest in the central United States. Observed mixing ratios of C₂-C₅ alkanes show enhancements over the central United States below 2 km. A nested GEOS-Chem simulation underpredicts observed C₃H₈ mixing ratios in the boundary layer over several U.S. regions, and the relative underprediction is not consistent, suggesting C₃H₈ emissions should receive more attention moving forward. Our decision to consider only C₄-C₅ alkane emissions as a single lumped species produces a geographic distribution similar to observations. Due to the increasing importance of oil and gas emissions in the United States, we recommend continued support of existing long-term measurements of C₂-C₅ alkanes. We suggest additional monitoring of C₂-C₅ alkanes downwind of northeastern Colorado, Wyoming, and western North Dakota to capture changes in these regions. The atmospheric chemistry modeling community should also evaluate whether chemical mechanisms that lump larger alkanes are sufficient to understand air quality issues in regions with large emissions of these species.

1. Introduction

The rise in oil prices caused domestic production of oil and gas to experience a rapid growth in the United States since 2005 (U.S. Energy Information Administration, 2017), increasing emission rates of many trace gases over oil and gas-producing basins (de Gouw et al., 2014; Kort et al., 2016). Development of, active production from, and abandonment of oil and gas wells emit volatile organic compounds (VOCs). These emissions impact climate (Brandt et al., 2014; Brantley et al., 2014; Franco et al., 2016; Mitchell et al., 2015; Roscioli et al., 2015), the formation of ozone and aerosols (Field et al., 2015; Guo, 2012; Koss et al., 2015; Pacsi et al., 2015; Phillips-Smith et al., 2017; Pusede & Cohen, 2012; Rappenglück et al., 2014), and human exposure to air toxics (Brantley et al., 2015; Halliday et al., 2016; Zielinska et al., 2014). Observations suggest that depending on the lifetime and emission rate of each species, the impact on atmospheric abundances of VOCs emitted by oil and gas sources can be substantial at local, regional, and global scales. For example, inside the Denver-Julesburg Basin, Gilman et al. (2013) estimated that oil and gas sources are the dominant source (72–96%) of regional C₂ to C₇ alkane emissions. Similarly, in the Uintah Basin, oil and gas leakage contributes 43–82% of observed abundances of C₂-C₅ alkanes (Helmig et al., 2014; Swarthout et al., 2015).

In the Marcellus shale region, multiple studies show that unconventional oil and gas production is responsible for recent positive trends in the observed abundances of methane (CH_4) and ethane (C_2H_6 ; Goetz et al., 2017; Peischl et al., 2015; Vinciguerra et al., 2015). In the Northern Hemisphere, annual growth rates of C_2H_6 abundances of 3–5%/year between 2009 and 2014 have been attributed to the recent increase of oil and gas extraction in North America (Franco et al., 2016; Helmig et al., 2016).

In the context of rapidly changing industrial activities and the fact that production is often driven by transitory economics, updating emission inventories for the U.S. oil and gas sector represents a challenge. In addition to the rapid growth of the oil and gas industry, there are a number of factors that make constraining VOC emissions from this industry difficult: (1) Natural gas composition varies with the type of reservoir (e.g., tight gas vs. shale gas; Kort et al., 2016; Tzompa-Sosa et al., 2017; Warneke et al., 2014); (2) Emissions depend on the stage (e.g., development, production or abandoned) of a well. Most of the VOC emissions occur during production (Pacsi et al., 2015), but emissions can continue for decades even after the well has been abandoned (Kang et al., 2014); (3) Emission inventories rely on activity factors and emission factors that represent typical emission rates for oil and gas wells. However, Brandt et al. (2016) found that in the United States 5% of the wells contribute over 50% of the total leakage volume of CH_4 . These emission outliers (so-called “superemitters”) are poorly understood and not represented in emission inventories; (4) National and state regulations vary with respect to in situ emission control technologies (U.S. Environmental Protection Agency, EPA, 2016a).

In this work, we examine C_2 – C_5 alkane emissions from the most recently updated 2011 National Emission Inventory (NEI), which includes updates over important oil-and-gas-producing basins and revised speciation profiles. We use those emissions to estimate the contribution to atmospheric abundances of C_2 – C_5 alkanes over the United States from this industry. There have been several modeling studies that have begun to explore this issue (Kort et al., 2016; Thompson et al., 2017). Also, we compare abundances of C_2 – C_5 to a suite of surface observations, column measurements, and aircraft profiles.

2. Methods

In order to investigate the oil and gas contribution to atmospheric abundances of C_2 – C_5 alkanes over the United States, we use emission fluxes from the model-ready version of the 2011v6.3 emissions modeling platform (more specifically the 2011ek modeling case) and incorporate them into the Goddard Earth Observing System global chemical transport model (GEOS-Chem). In this section, we explain the regridding and unit conversion process of the 2011v6.3 emissions modeling platform fluxes, the creation of year-round daily emission fluxes for the year 2011, and the implementation of year-round daily emission fluxes into GEOS-Chem.

2.1. Updated 2011NEI Emission Fluxes Over the United States

In the United States, the NEI is released every three years. It is based on activity data from state and local agencies. Here, we use an updated version of the 2011NEI that is part of the EPA 2011v6.3 emissions modeling platform (U.S. EPA, 2016b; <https://www.epa.gov/air-emissions-modeling/2011-version-63-technical-support-document>). Specifically, the modeling case used for the emissions is from the initial version of the 2011v6.3 platform and is also known as “2011ek.” This platform uses the Carbon Bond Mechanism version 6 (CB06) to compute emissions for use as inputs to chemical transport models that require hourly and gridded emissions of chemical species. Relevant to this study, CB06 includes chemical reactions to treat explicit VOC species, such as C_3H_8 , benzene, and acetone. In previous model versions, these explicit species were lumped in the paraffin (PAR) species. This work uses specific emissions of propane, benzene, and acetone for all model simulations (see section 2.2). Also, the handling of PAR species in our GEOS-Chem model simulations is explained in section 2.2.

In the 2011v6.3 modeling platform, oil and gas emission sources are divided into point and nonpoint sources. Oil and gas point sources include extraction and distribution of oil and natural gas and pipeline transportation and support activities for oil and gas operations. Nonpoint oil and gas sources include drill rigs, work-over rigs, artificial lifts, hydraulic fracturing engines, pneumatic pumps, and other devices, storage tanks, flares, truck loading, compressor engines, and dehydrators. The 2011v6.3 platform is expected to better represent the spatial distribution, amount, and type of species emitted from oil and gas sources due to the

Table 1
Characteristics of Emission Sources From the 2011v6.3 Platform Emissions Data Set Included in This Work

Source category	Emission sector	Temporal resolution	Number of files
Point	Electric generating units	daily	365
	Point oil and gas	day-of-week	64
	Other point sources	day-of-week	64
Nonpoint	Agricultural ammonia	daily	365
	Commercial marine vessels	monthly	12
	Nonpoint oil and gas	weekly	100
	Other nonpoint sources	weekly	100
	Railroads	monthly	12
	Residential wood combustion	daily	365
On road		daily	365
Nonroad		day-of-week	64

Note. Day-of-week and weekly temporal resolutions include emission files for holidays and the consecutive day after each holiday.

incorporation of updates over important oil-and-gas-producing basins and speciation profiles based on the Western Regional Air Partnership (WRAP, www.wrapair2.org). WRAP is a voluntary partnership of states, tribes, federal land managers, local air agencies, and the U.S. EPA within the contiguous United States (CONUS) West plus North and South Dakota. The WRAP region encompasses several major U.S. natural gas production basins. Incorporating WRAP data into the 2011v6.3 platform is part of multiple efforts by the EPA to revisit and understand the dynamic nature of oil and gas emissions.

2.1.1. Regridding and Unit Conversion Process of Emission Fluxes

The air quality model-ready emissions in the platform data set contain daily files with hourly primary emission fluxes in moles per second (mol/s) on a curvilinear grid at 12-km × 12-km horizontal resolution for all states inside the CONUS (U.S. EPA, 2017). These model-ready emission files were created using the Sparse Matrix Operator Kernel Emissions modeling system (SMOKE, <http://www.smoke-model.org/>) version 3.7. We converted the emission fluxes using mass conservative interpolation into kilograms per square meter per second (kg/m²/s) and

regridded them onto a rectilinear grid at a 0.1° longitude by 0.1° latitude resolution (equivalent to approximately 8 km × 11 km over the United States). We used the Earth System Modeling Framework software to interpolate from the curvilinear SMOKE data grid to the rectilinear GEOS-Chem grid. Table 1 shows a list of the 2011v6.3 platform anthropogenic emission sources considered in this study.

2.1.2. Creation of Year-Round Daily Emission Fluxes

Each emission sector in the 2011v6.3 platform has daily emission flux files, presented in one out of four different temporal resolutions: daily, according to the day-of-week, weekly, and monthly. Sectors with daily temporal resolution have hourly emissions computed for every day of 2011. Sectors with a temporal approach according to the day-of-week have hourly emissions for four representative days per month: a Saturday, Sunday, Monday, and weekday (representing Tuesday through Friday). For sectors with a weekly temporal approach, hourly emissions are computed for all 7 days of one representative week in each month. Additionally, the day-of-week and weekly temporal resolutions include emission files for holidays and the consecutive day after each holiday. Table 1 summarizes the temporal resolution approach for each of the emission sectors. For the seven sectors without a daily temporal resolution, year-round daily emission files were created by reproducing the emission flux files according to the temporal resolution of each sector. For example, each emission sector with a monthly temporal resolution had 12 emission flux files; thus, each monthly file was reproduced according to the number of days of the month it represented.

The complete emissions data set in 2011v6.3 platform contains additional emission sources and species than the ones considered in this work. Thus, hereafter we will refer to the implemented emissions from 2011v6.3 platform as updated 2011NEI emissions.

2.2. GEOS-Chem Simulations

We conducted two nested simulations (0.5° × 0.6°) over North America (40° to 140°W, 10° to 70°N) using the 3-D chemical transport model GEOS-Chem version 10-01 (Bey et al., 2001, <http://www.geos-chem.org>) for the year 2011. The GEOS-Chem model was driven by off-line GEOS-5 assimilated meteorological fields (<https://gmao.gsfc.nasa.gov/GEOS/>) with 47 vertical levels. Global simulations at 2° × 2.5° resolution with a spin-up of 18 months were used as boundary conditions for the nested simulations. The emissions and injection time steps were set to 20 min; the transport time step was set to 10 min.

In our baseline simulation, we implemented the updated 2011NEI emission fluxes into GEOS-Chem using the stand-alone software component for computing emissions, Harvard-National Aeronautics and Space Administration Emissions Component (HEMCO) version 1.1.005 (Keller et al., 2014). Over the CONUS, all anthropogenic and biofuel emissions were derived from the updated 2011NEI. Outside the CONUS, we used anthropogenic emissions from the Emissions Database for Global Atmospheric Research (EDGAR v4.2), and VOC emissions from the Reanalysis of the Tropospheric chemical composition (RETRO) emission inventory, except for C₂H₆ and C₃H₈, for which we used the Tzompa-Sosa et al. (2017) and Xiao et al. (2008)

Table 2
Configuration of Emission Inventories in Our Baseline Simulation

Emission inventory	Region	Base year	Species in GEOS-Chem ^b
Anthropogenic Updated 2011NEI	CONUS	2011	ACET, ALD2, ALK4, BCPI, BCPO, BENZ, C ₂ H ₄ , C ₂ H ₆ , C ₃ H ₈ , CO, EOH, FORM, HONO, MACR, MEK, MOH, NH ₃ , NO, NO ₂ , OCPI, OCPO, PRPE, RCHO, SO ₂ , SO ₄ , TOLU, and XYLE
BRAVO	Northern Mexico	1999	CO, NO, SO ₂ , and SO ₄
CANADA	Canada	2002 ^a	CO, NO, SO ₂ , and SO ₄
EMEP	Europe	2008	NH ₃
MIX	Asia	2011	CO, NH ₃ , NO, and SO ₂
EDGAR	global	2000	ALD2, ALK4, MEK, and PRPE
Tzompa-Sosa et al. (2017)	global	2010 ^a	ALD2, ALK4, CH ₂ O, CO, NH ₃ , NO, SO ₂ , SO ₄ , MEK, and PRPE
Xiao et al. (2008)	global	2008 ^a	CO, NAP, NH ₃ , NO, SO ₂ , and SO ₄
RETRO	global	2010	C ₂ H ₆
		1985	C ₃ H ₈
		2000	ACET, ALD2, ALK4, BENZ, CH ₂ O, C ₂ H ₂ , C ₂ H ₄ , MEK, PRPE, TOLU, and XYLE
Biofuel Updated 2011NEI	CONUS	2011	ACET, ALD2, ALK4, BCPI, BCPO, BENZ, C ₂ H ₄ , C ₂ H ₆ , C ₃ H ₈ , CO, EOH, FORM, HONO, MACR, MEK, MOH, NH ₃ , NO, NO ₂ , OCPI, OCPO, PRPE, RCHO, SO ₂ , SO ₄ , TOLU, and XYLE
Yevich and Logan (2003)	global, except the CONUS	1985	ACET, ALD2, ALK4, BENZ, CH ₂ O, C ₂ H ₂ , C ₂ H ₄ , C ₃ H ₈ , CO, GLYC, GLYX, HAC, MEK, MGLY, NAP, NO, PRPE, SO ₂ , TOLY, and XYLE
GEIA	global	1998	NH ₃
Tzompa-Sosa et al. (2017)	global	2010	C ₂ H ₆
Shipping			
EMEP	Europe	2011	CO, NO, and SO ₂
ARCTAS	global	2008	SO ₂
ICOADS	global	2002	CO and NO
Aviation			
AEIC	global	2005	ACET, ALD2, ALK4, BC, CH ₂ O, C ₂ H ₆ , C ₃ H ₈ , CO, MACR, NO, SO ₂ , SO ₄ , OC, PRPE, and RCHO
Natural sources			
GEOS-Chem default	global	2000	NO
		1985	DMS
		2009	SO ₂
GEIA	global	1990	NH ₃

Note. 1. Over the CONUS, all anthropogenic and biofuel emissions in the baseline simulation come from the updated 2011NEI. 2. Unless otherwise noted, the simulation uses the same year as the base year for the 2011 simulation. GEIA = Global Emissions Initiative; CONUS = contiguous United States; EDGAR = Emissions Database for Global Atmospheric Research.

^aProjected to 2010 using GEOS-Chem default annual scaling factors. ^bSpecies in GEOS-Chem can be found in http://wiki.seas.harvard.edu/geos-chem/index.php/Species_in_GEOS-Chem.

emission inventories, respectively. We also include regional anthropogenic emission inventories for northern Mexico (Kuhns et al., 2003), Canada (<https://www.canada.ca/en/environment-climate-change/services/national-pollutant-release-inventory/tools-resources-data.html>), Europe (<http://www.ceip.at/>), and Asia (<http://meicmodel.org/dataset-mix.html>). Non-U.S. biofuel emissions were from the Yevich and Logan (2003) emission inventory, with two exceptions. (1) We used ammonia (NH₃) emissions from the Global Emissions Initiative and (2) C₂H₆ emissions from Tzompa-Sosa et al. (2017). Shipping, aviation, and natural sources are expected to make minor contributions to the emissions of C₂-C₅ alkanes; the default global data sets incorporated into GEOS-Chem were used for these sectors. Table 2 shows the summary of the emission inventories that we used in the baseline simulation.

For the second simulation (hereafter updated 2011NEI: OG off), we maintained the same configuration of emission inventories as the baseline simulation, but we turned off the updated 2011NEI emissions of greater than or equal to C₂ alkanes from the oil and gas sector. We used this simulation to investigate the contribution of oil- and gas-related activities to the abundance of the greater than or equal to C₂ alkanes over the CONUS.

The alkane speciation used in GEOS-Chem was originally based on the Lurmann et al. (1986) condensed gas phase chemical mechanism. The current mechanism in GEOS-Chem treats C_3H_8 and C_2H_6 as explicit species. Greater than or equal to C_4 alkanes are lumped into one tracer, originally named ALKA in Lurmann et al. (1986), and currently named ALK4 in GEOS-Chem. The rate constant in GEOS-Chem associated with the reaction of OH with ALK4 is based on the absolute rate coefficient of butane ($9.1 \times 10^{-12} e^{(-405/T)} \text{ cm}^3 \cdot \text{molecule}^{-1} \cdot \text{s}^{-1}$; Atkinson et al., 2006), but is used to represent the chemistry of all greater than or equal to C_4 alkanes. Both of our simulations have a global annual mean tropospheric mass-weighted OH concentration of $1.3 \times 10^6 \text{ molecule/cm}^3$, which is very close to the upper bound of previous model studies in the literature (Naik et al., 2013; Voulgarakis et al., 2013). In this study, we consider ALK4 specifically as n-butane, i-butane, n-pentane, and i-pentane (hereafter referred to as C_4 - C_5 alkanes), rather than a more inclusive greater than or equal to C_4 alkanes. Thus, one obvious challenge with the model-observation comparison that we present later in the paper is the use of a single reaction rate for C_4 - C_5 alkanes. As explained in section 2.1, 2011v6.3 platform emissions of PAR species include alkanes. We assigned a fraction of PAR to C_4 - C_5 alkane species based on Simon et al. (2010). They summarize the 50 VOCs with the largest emissions over the United States; for an example day, C_4 - C_5 alkanes correspond to 36% of these emissions over the United States. Thus, we set ALK4 emissions as 36% of the total PAR emitted species. The remaining reactive carbon in the PAR species is not considered here. Omitting such a large fraction of reactive carbon limits our ability to provide a full view of the impact of oil and gas operations and urban activities on atmospheric composition. This is a known limitation to our approach. However, we investigated the impact of attributing 100% of PAR to ALK4 versus 36% of PAR to ALK4 on ALK4 lifetime. Omitting such a large fraction of carbon changes the lifetime of ALK4 over the United States by <5%. As discussed in section 4, we suggest that the addition of a new GEOS-Chem tracer for C_6 - C_8 alkanes, which based on the 50 VOCs with largest emissions over the United States (Simon et al., 2010), accounts for ~40% of PAR. Thus, adding such fraction of the remaining reactive carbon from the PAR species could provide a better estimate of the full impact of the emissions from this sector.

The GEOS-Chem mechanism does not include other paraffin compounds, such as alkynes, and higher aromatic VOCs that have also been found in high abundances (compared to background values) over oil and gas basins (Abeleira et al., 2017; Gilman et al., 2013; Helmig et al., 2014; Pétron et al., 2012, 2014; Swarthout et al., 2013, 2015; Thompson et al., 2014; Zielinska et al., 2014). Additionally, our model simulations do not include tropospheric chlorine chemistry; thus, reaction with OH is the only tropospheric sink of C_2 - C_5 alkane species. Sherwen et al. (2016) used the same initial GEOS-Chem version, but they added tropospheric halogen chemistry (Cl, Br, and I). In their study, adding a chlorine sink term led to decreases in the tropospheric global burdens of C_2H_6 , C_3H_8 , and greater than or equal to C_4 alkanes of 19%, 14%, and 12%, respectively. However, global tropospheric burden changes are heterogeneous, and in general, they are lower over land compared to oceans. At the surface over the United States, the annual average changes are smaller (typically <10% for C_2H_6 and less for C_3H_8 , and greater than or equal to C_4 alkanes; see Sherwen et al., 2016, Figure 19). The inclusion of halogen chemistry would decrease the O_3 burden and thus the OH burden as well. This would increase the lifetimes of C_2H_6 , C_3H_8 , and greater than or equal to C_4 alkanes against OH oxidation. Given that the inclusion of updated 2011NEI emissions in our model produces significant increases in C_2 - C_5 alkane fluxes over the United States compared to the emission inventory used by Sherwen et al. (2016), a comprehensive understanding of these two model developments would require additional model simulations.

3. Results and Discussion

3.1. Contribution of the Oil and Gas Sector to Emissions of C_2 - C_5 Alkanes

3.1.1. Ethane and Propane

The oil and gas sector emits C_2H_6 and C_3H_8 primarily due to leakage during the production, processing, and transportation of natural gas (Gilman et al., 2013; Kort et al., 2016; Pétron et al., 2012; Roest & Schade, 2017). Trace amounts of C_2H_6 and C_3H_8 can also be produced during hydrocarbon combustion processes (Basevich et al., 2012; Gomer & Kistiakowsky, 1951; Sangwan et al., 2015; Thynne, 1962). In the updated 2011NEI, total emissions of C_2H_6 and C_3H_8 are dominated by oil and gas sources (point sources—e.g., oil and gas extraction, distribution, and pipelines—and nonpoint sources—e.g., flares, drill, and workover rigs), with an

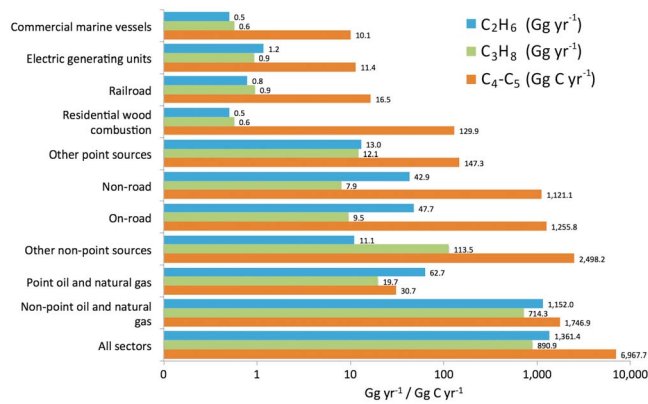


Figure 1. Updated 2011NEI emissions of C₂H₆, C₃H₈, and C₄-C₅ alkanes by sector. C₄-C₅ alkanes are presented as 36% of PAR emissions. Units for C₂H₆ and C₃H₈ are in gigagrams per year, and units for C₄-C₅ alkanes are presented in gigagrams of carbon per year.

estimated contribution to total anthropogenic emissions for the United States of 89% and 82%, respectively (Figure 1). The remaining percentage of C₂H₆ and C₃H₈ emissions is distributed among other sources such as vehicles and residential wood combustion. We note that from the two oil and gas sectors considered, nonpoint sources are the biggest contributors, accounting for 95% and 97% of the total oil and gas contribution estimate.

The total updated 2011NEI emissions of C₂H₆ from the present study are 15% lower than the Tzompa-Sosa et al. (2017) C₂H₆ emission inventory estimate, which was calculated by scaling C₂H₆ emissions of 2011NEI version 1 (2011NEIv1) by a factor of 1.4 based on a comparison to existing observations. It is important to note that the 2011NEIv1 did not contain updates over oil and gas basins based on the WRAP (the updated 2011NEI used here includes the WRAP data), causing oil and gas regions like the Uintah basin to have minimal C₂H₆ emission fluxes. In this region, where studies have found important C₂H₆ emission enhancements (Helmig et al., 2014; Koss et al., 2015; Warneke et al., 2014), emission fluxes from oil and gas sources in 2011NEIv1 are close to 0; thus, upward scaling by 1.4 still results in a small flux. Thus, if the scaling in Tzompa-Sosa et al. (2017) were applied in this study, the result would be a different spatial distribution and amount of emission fluxes compared to the updated 2011NEI used here. Lastly, we notice that between 2011NEIv1 and the updated 2011NEI used in this work, emissions of C₃H₈ have higher emission flux increases compared to C₂H₆. The highest emission fluxes occur over oil and gas regions in the central United States, with increases of up to 300 ng·m⁻²·s⁻¹.

3.1.2. C₄-C₅ Alkanes

Over the last decade, leakage from oil and gas sources has become an important contributor to the emissions of C₄-C₅ alkanes (Gilman et al., 2013; Johansson et al., 2014; Roest & Schade, 2017; Swarthout et al., 2013, 2015), which historically were dominated by automobile combustion, and fugitive emissions from gasoline and diesel distribution (Lee et al., 2006; Schauer et al., 2002). Thus, urban areas are the locations where enhancements of C₄-C₅ alkanes are commonly observed (Aceves & Grimalt, 1993; Bi et al., 2005; Lee et al., 2006). Rossabi and Helmig (2018) recently used data collected between 2001 and 2015 over the United States to show a predominantly decreasing trend in C₄-C₅ alkanes surface mixing ratios, but they found a relative increase in the predominance of the n-isomers. They attributed this pattern to changes in isomeric ratios in gasoline sector emissions and emissions from the oil and gas industry. The emergence of U.S. oil and gas development as a larger source of C₄-C₅ alkanes has increased their atmospheric abundances in areas with low population density (Gilman et al., 2013; Pétron et al., 2014; Warneke et al., 2014). Gilman et al. (2013) estimated that the mean oil and gas contribution to C₄-C₅ alkane emissions in northeastern Colorado is 93–96%. Based on the updated 2011NEI emissions (Figure 1), we estimate that oil and gas sources (including both point and nonpoint sources) over the CONUS are the third most important emission source of C₄-C₅ alkanes with an annual contribution of 26% of the total emissions.

3.1.2. C₄-C₅ Alkanes

3.2. Geographical Distribution of Oil and Gas C₂-C₅ Alkane Emissions and Its Contribution to U.S. Total Anthropogenic Emissions

In the United States, emissions of C₂H₆ and C₃H₈ are mainly clustered inside oil and gas basins, where the contribution of the oil and gas sector to total anthropogenic emissions is >90% (Figures 2a and 2b). For C₄-C₅ alkanes, the emissions occur not only inside oil and gas basins but also in urban areas due to the importance of other fossil fuel sources. The contribution of urban sources to total emissions of C₄-C₅ alkanes over oil-and-gas-producing regions reduces the overall percentage contribution of oil and gas sources (Figure 2c).

3.2. Geographical Distribution of Oil and Gas C₂-C₅ Alkane Emissions and Its Contribution to U.S. Total Anthropogenic Emissions

A comparison between regional emissions of C₂H₆, C₃H₈, and C₄-C₅ alkanes shows that the central region of the United States is the most important contributor to total CONUS C₂-C₅ alkane emissions in 2011, contributing ~70% of C₂H₆ and C₃H₈ total CONUS emissions, and ~40% of the emissions of C₄-C₅ alkanes (Figure 3). The central region fully encompasses four U.S. oil and gas basins: Eagle Ford (Texas), Permian (Texas), Niobrara (Colorado and Wyoming), and Bakken (North Dakota). This estimate is likely to be

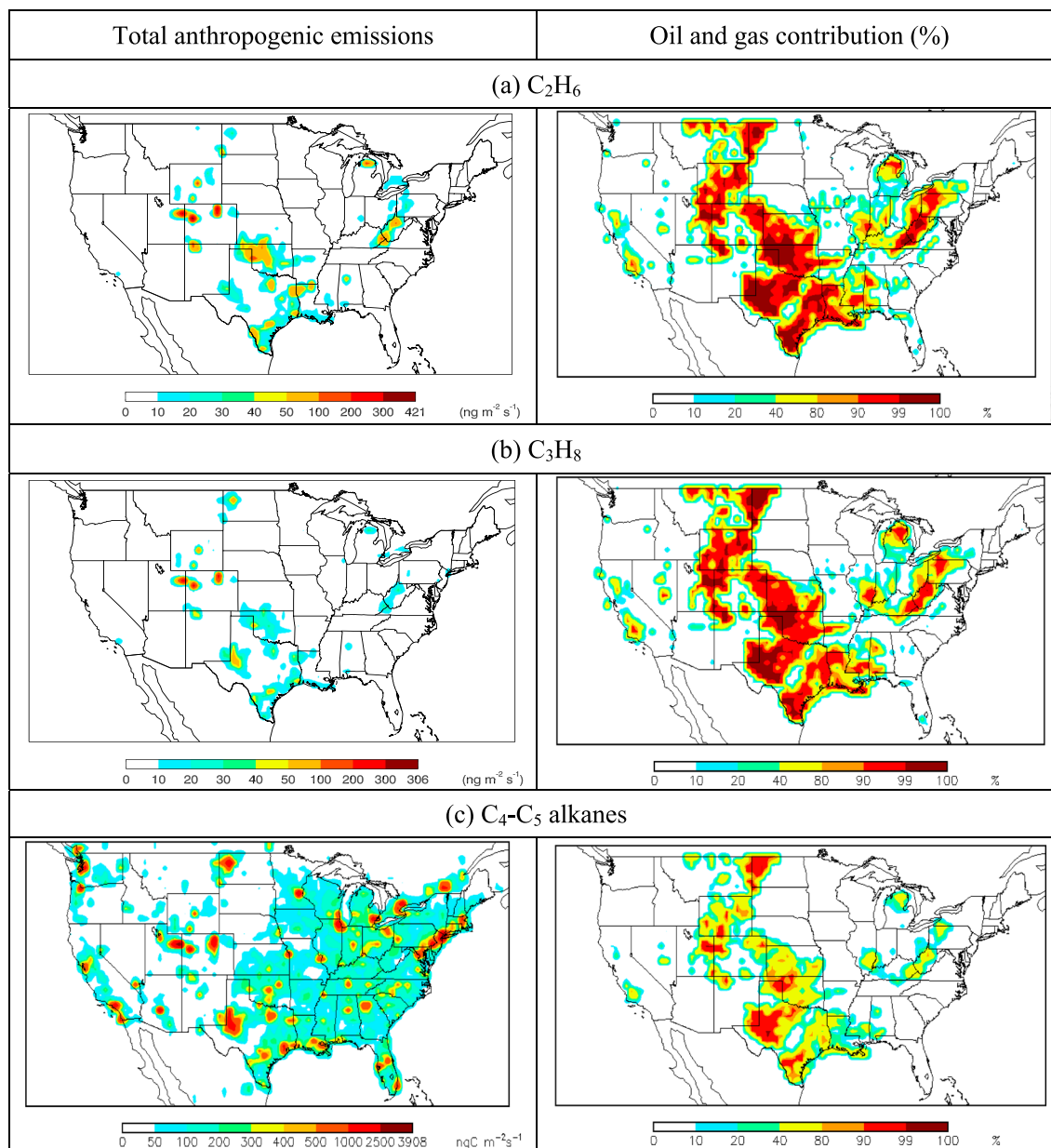


Figure 2. (left column) Spatial distribution of anthropogenic emissions of C_2H_6 , C_3H_8 , and C_4-C_5 alkanes. (right column) Spatial distribution of the contribution of oil and gas emissions to total anthropogenic emissions of C_2H_6 , C_3H_8 , and C_4-C_5 alkanes. C_2-C_5 alkane emissions data from the updated 2011NEI. C_4-C_5 alkanes are presented as 36% of PAR emissions.

higher for years later than 2011 for C_2H_6 due to the massive increase in oil and gas exploitation in the Bakken basin (Kort et al., 2016; Peischl et al., 2016).

3.3. Model Comparison to Observations and Oil and Gas Contribution to Atmospheric Abundances of C_2-C_5 Alkanes

We compare 2011 abundances of C_2H_6 , C_3H_8 , and C_4-C_5 alkanes from a GEOS-Chem simulation to a suite of observations over North America (Table 3 and Figure 4). To the best of our knowledge, this constitutes the largest compendium of C_2-C_5 alkane observations compared to model output for this region. Also, we estimate the contribution of oil and gas to atmospheric abundances of C_2H_6 , C_3H_8 , and C_4-C_5 alkanes by turning

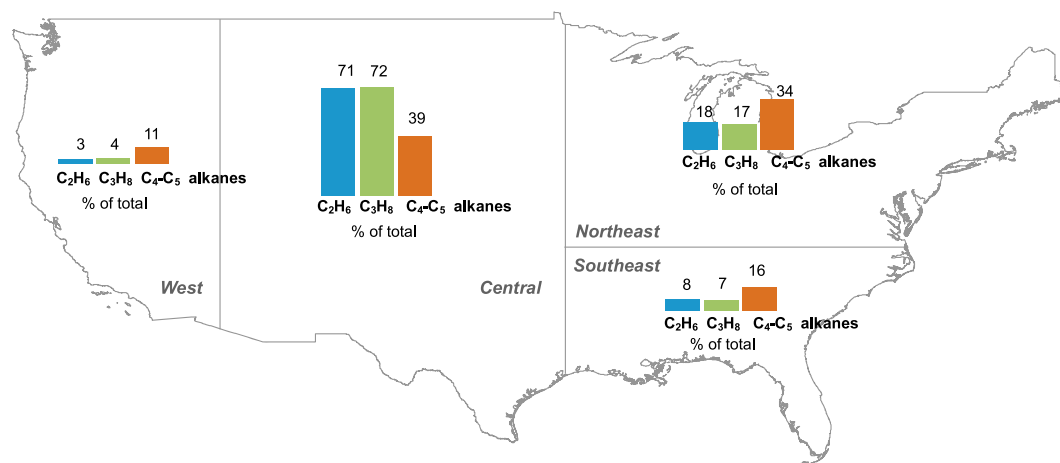


Figure 3. Regional contributions (as %) to U.S. total anthropogenic emissions of C₂H₆, C₃H₈, and C₄-C₅ alkanes. C₂-C₅ alkane emissions data from the updated 2011NEI. C₄-C₅ alkanes are presented as 36% of PAR emissions.

off the emissions of these species from the oil and gas sector in a separate GEOS-Chem simulation (updated 2011NEI: OG off).

3.3.1. Comparison to Ground-Based FTIR C₂H₆ Column Observations

In this section, we compare 2011 C₂H₆ total columns derived from ground-based Fourier transform infrared (FTIR) solar observations at the Boulder and Toronto stations to GEOS-Chem simulated C₂H₆ total columns for our two emission scenarios (Figure 5). The C₂H₆ total columns were determined at both sites following the methodology described in Franco et al. (2015). The latter paper further provides information on the typical systematic and random uncertainties affecting the column measurements. The first emission scenario considers all emissions and sectors from the updated 2011NEI. In the second emission scenario, C₂H₆ emissions from the oil and gas industry are turned off (updated 2011NEI: OG off). Finally, the oil and gas contribution to C₂H₆ total columns is calculated by subtracting the results of the second scenario (updated 2011NEI: OG off) from those of the first scenario (updated 2011NEI).

At the Boulder station, C₂H₆ emissions from the updated 2011NEI reproduce observed C₂H₆ total columns outside of winter months. A difference of $\sim 0.2\text{--}1 \times 10^{16}$ molecules/cm² is observed during the winter season (including November). At the Toronto station, modeled updated 2011NEI C₂H₆ emissions underestimate (on average by $\sim 0.5 \times 10^{16}$ molecules/cm²) the observed C₂H₆ total column throughout the year 2011. We note that as shown in Table 2, our simulation does not include recent updates to C₂H₆ emission fluxes made by Environment and Climate Change Canada. The difference in observed and modeled C₂H₆ total columns might be due to a combination of underestimated urban C₂H₆ leakage from natural gas delivery and end use, residential wood combustion, and the higher resolution ($0.5^\circ \times 0.6^\circ$) analysis made in this study using $2^\circ \times 2.5^\circ$ C₂H₆ emissions derived by Tzompa-Sosa et al. (2017). The coarser resolution of the C₂H₆ emissions over Toronto limits the ability of our higher-resolution model simulation to capture local enhancements. The total C₂H₆ columns observed and produced by both emission scenarios over Toronto are larger than over Boulder. Considering that the column measurements are sensitive to the whole troposphere and lower stratosphere, the column difference between Toronto and Boulder can be explained by the altitude difference between both stations (~ 1.5 km). Another possible explanation of the column difference is the latitudinal gradient in C₂H₆, with higher abundances toward the Arctic (Helmig et al., 2016; Simpson et al., 2012).

There is a greater contribution to modeled total C₂H₆ columns from emissions from the oil and gas sector ($\sim 0.7 \times 10^{16}$ molecules/cm²) at the Boulder station compared to the Toronto station ($\sim 0.4 \times 10^{16}$ molecules/cm²). This finding is consistent with results presented in Franco et al. (2016) for the 2009–2014 period. Among six FTIR stations (including Toronto) located at different latitudes across the Northern Hemisphere, they showed that the Boulder station had the highest rate of change in the C₂H₆ total column over this time period, presumably associated with the oil and gas development in the central United States. The high contribution of the oil and gas sector over Boulder is also shown in results from this study (Figure 2).

Table 3
Observations From Surface Sites and Airborne Campaigns, Ordered by Type and Date

2011 FTIR column measurements				
Species	Site	Location	Period	Reference
C ₂ H ₆	Toronto, Ontario, Canada	79.4°W, 43.6°N	January–December 2011	Wiacek et al. (2007)
C ₂ H ₆	Boulder, Colorado, USA	105.3°W, 40.4°N	January–December 2011	Hannigan et al. (2009)
Aircraft campaigns				
Species	Field campaign	Region	Period	Reference
C ₂₋₅	ARCTAS	110° to 126°W, 30° to 50°N	April, June–July 2008	Simpson et al. (2010) Simpson et al. (2011)
C ₂₋₅	HIPPO	90° to 116°W, 25° to 50°N	June–September 2011	Wofsy et al. (2012)
C ₂₋₅	SEACR ⁴ S	80° to 126°W, 25° to 50°N	August–September 2013	Blake et al. (2014) Schauffler et al. (2014)
C ₂₋₅	FRAPPÉ	101° to 109°W, 38° to 46°N	July–August 2014	Richter et al. (2015)
2011 Surface flask measurements from National Oceanic and Atmospheric Administration/Institute of Arctic and Alpine Research Global VOC Monitoring Program				
Species	Site	Location	Period	Website
C ₂₋₅	Key Biscayne, Florida (KEY), USA	80.16°W, 25.67°N	January–December 2011	https://www.esrl.noaa.gov/gmd/dv/data/
C ₂₋₅	Park Falls, Wisconsin (LEF), USA	90.27°W, 45.95°N	January–December 2011	
C ₂₋₅	Southern Great Plains, Oklahoma, (SGP), USA	97.5°W, 36.8°N	January–December 2011	
C ₂₋₅	Trinidad Head, California (THD), USA	124.15°W, 41.05°N	January–December 2011	
C ₂₋₅	Wendover, Utah (UTA), USA	113.72°W, 39.9°N	January–December 2011	
2011 Surface flask measurements from Photochemical Assessment Monitoring Stations				
Species	Site	Location	Period	Website
C ₂₋₅	Baltimore, Maryland (BAL), USA	76.6°W, 39.3°N	June–August 2011	https://www.airnowtech.org
C ₂₋₅	Boston, Massachusetts (BOS), USA	71.1°W, 42.4°N	June–August 2012	
C ₂₋₅	El Paso, Texas (ELP), USA	106.4°W, 31.8°N	January–December 2011	
C ₂₋₅	Gary, Indiana (GAR), USA	87.3°W, 41.6°N	June–December 2011	
C ₂₋₅	Houston, Texas (HOU), USA	95.4°W, 29.8°N	January–December 2011	
C ₂₋₅	Los Angeles, California (LAX), USA	118.3°W, 34.1°N	January–December 2011	
C ₂₋₅	Philadelphia, Pennsylvania (PHI), USA	75.2°W, 40°N	May–October 2011	
C ₂₋₅	Atlanta, Georgia (SDK), USA	84.4°W, 33.8°N	June–August 2011	
C ₂₋₅	Springfield, Massachusetts (SPR), USA	72.5°W, 42.1°N	June–August 2011	
Surface observations				
Species	Site	Location	Period	Reference
C ₄₋₅	Houston Ship Channel, Texas (HSC), USA	95.03°W, 29.65°N	September 2006	Johansson et al. (2014)
C ₃₋₅	San Francisco, California (STR), USA	122.45°W, 37.76°N	June–August 2007–2010	Pétron et al. (2012) ¹
C ₃₋₅	Walnut Grove, California (WGC), USA	121.49°W, 38.26°N	June–August 2007–2010	Pétron et al. (2012) ¹
C ₃₋₅	Moody, Texas (WKT), USA	97.33°W, 31.32°N	June–August 2007–2010	Pétron et al. (2012) ¹
C ₃₋₅	Park Falls, Wisconsin (LEF), USA	90.27°W, 45.93°N	June–August 2007–2010	Pétron et al. (2012) ¹
C ₅	Barnett Shale, Texas (BST), USA	97.42°W, 33.27°N	May 2010	Zielinska et al. (2014)
C ₃₋₅	Boulder Atmospheric Observatory, Colorado (BAO), USA	105.01°W, 40.05°N	August 2007 to April 2010	Pétron et al. (2012)
C ₂₋₅	Boulder Atmospheric Observatory, Colorado (BAO), USA	105.01°W, 40.05°N	February–March 2011	Gilman et al. (2013)
C ₂₋₅	Boulder Atmospheric Observatory, Colorado (BAO), USA	105.01°W, 40.05°N	February–March 2011	Swarthout et al. (2013)
C ₂₋₅	Beaumont Downtown, Texas (BDT), USA	94.07°W, 30.04°N	January–December 2011	TCEQ (2012) ²
C ₂₋₅	Cesar Chavez HS, Texas (CCH), USA	95.25°W, 29.68°N	January–December 2011	TCEQ (2012) ²
C ₂₋₅	Channelview, Texas (CNV), USA	95.13°W, 29.8°N	January–December 2011	TCEQ (2012) ²
C ₂₋₅	Clinton, Texas (CLT), USA	95.26°W, 29.73°N	January–December 2011	TCEQ (2012) ²
C ₂₋₅	Corpus Christi Oak Park, Texas (CCO), USA	97.43°W, 27.8°N	January–December 2011	TCEQ (2012) ²
C ₂₋₅	Corpus Christi Palm, Texas (CCP), USA	97.42°W, 27.8°N	January–December 2011	TCEQ (2012) ²
C ₂₋₅		97.54°W, 27.83°N	January–December 2011	TCEQ (2012) ²

Table 3 (continued)

Species	Site	Location	Period	Reference
	Corpus Christi Solar Estates, Texas (CCS), USA			
C ₂₋₅	Dallas Hinton, Texas (DHT), USA	96.86°W, 32.82°N	January–December 2011	TCEQ (2012) ²
C ₂₋₅	Danciger, Texas (DNG), USA	95.76°W, 29.14°N	January–December 2011	TCEQ (2012) ²
C ₂₋₅	Decatur Thompson, Texas (DTS), USA	97.58°W, 33.22°N	January–December 2011	TCEQ (2012) ²
C ₂₋₅	Deer Park, Texas (DPK), USA	95.13°W, 29.67°N	January–December 2011	TCEQ (2012) ²
C ₂₋₅	Dish Airfield, Texas (DAF), USA	97.3°W, 33.13°N	January–December 2011	TCEQ (2012) ²
C ₂₋₅	Eagle Mtn Lake, Texas (EML), USA	97.48°W, 32.99°N	January–December 2011	TCEQ (2012) ²
C ₂₋₅	El Paso Chamizal, Texas (EPC), USA	106.46°W, 31.77°N	January–December 2011	TCEQ (2012) ²
C ₂₋₅	El Paso Delta, Texas (EPD), USA	106.41°W, 31.76°N	January–December 2011	TCEQ (2012) ²
C ₂₋₅	Everman Johnson Park, Texas (WJP), USA	97.29°W, 32.62°N	January–December 2011	TCEQ (2012) ²
C ₂₋₅	Flower Mound, Texas (FWM), USA	97.13°W, 33.05°N	January–December 2011	TCEQ (2012) ²
C ₂₋₅	Fort Worth NW, Texas (FWN), USA	97.36°W, 32.81°N	January–December 2011	TCEQ (2012) ²
C ₂₋₅	HRM3, Texas (HRM), USA	95.18°W, 29.76°N	January–December 2011	TCEQ (2012) ²
C ₂₋₅	Lake Jackson, Texas (LJK), USA	95.47°W, 29.04°N	January–December 2011	TCEQ (2012) ²
C ₂₋₅	Lynchburg Ferry, Texas (LBF), USA	95.08°W, 29.76°N	January–December 2011	TCEQ (2012) ²
C ₂₋₅	Milby Park, Texas (MPK), USA	95.26°W, 29.71°N	January–December 2011	TCEQ (2012) ²
C ₂₋₅	Nederland HS, Texas (NDL), USA	94.01°W, 29.98°N	January–December 2011	TCEQ (2012) ²
C ₂₋₅	Odessa Hays, Texas (OHY), USA	102.34°W, 31.84°N	January–December 2011	TCEQ (2012) ²
C ₂₋₅	Texas City 34th St., Texas (TXC), USA	94.95°W, 29.41°N	January–December 2011	TCEQ (2012) ²
C ₂₋₅	Wallisville Rd, Texas (WVR), USA	94.99°W, 29.82°N	January–December 2011	TCEQ (2012) ²
C ₂₋₅	Hickory, Pennsylvania (HKY), USA	80.30°W, 40.30°N	July 2012	Swarthout et al. (2015)
C ₂₋₅	Racoon Creek State Park, Pennsylvania (RCS), USA	80.50°W, 40.50°N	July 2012	Swarthout et al. (2015)
C ₂₋₅	Erie, Colorado (ERC), USA	105.05°W, 40.05°N	March–June 2013	Thompson et al. (2014)
C ₂₋₅	Boulder Atmospheric Observatory, Colorado (BAO), USA	105.01°W, 40.05°N	March–May, July– September, 2015	Abeleira et al. (2017)

Note. C₄ and C₅ observations only include n-C₄H₁₀ and n-C₅H₁₂.

Furthermore, from the four regions analyzed in section 3.3.3 (Figure 10), the region where the Boulder station is located shows the highest percentage contribution from the oil and gas sector to total abundances of C₂–C₅ alkanes throughout the troposphere.

3.3.2. Comparison to Surface Flask Observations

In this section, we compare 2011 simulated alkane mixing ratios with and without oil and gas sources (blue and red lines, respectively in Figure 6) to measured C₂–C₅ surface mixing ratios from samples collected at selected U.S. stations (Table 3) from the National Oceanic and Atmospheric Administration Global Greenhouse Gas Reference Network stations are ordered from higher to lower latitudes due to the observed strong latitudinal gradient of C₂–C₅ alkane abundances (Helmig et al., 2016; Simpson et al., 2012). Differences between our simulations with and without emissions of C₂H₆ and C₃H₈ from the oil and gas sector suggest that the SGP station was more impacted by emissions from this industry compared to the rest of the stations throughout 2011. The estimated annual oil and gas source contributions to surface C₂H₆ and C₃H₈ mixing ratios at the SGP station are 86% for both species. The higher oil and gas impact at the SGP station is expected because it is located inside an oil and gas region. Typical i-pentane/n-pentane ratio for regions dominated by emissions from the oil and gas sector range from 0.89–1.10 (Gilman et al., 2013). The calculated 2011 i-pentane/n-pentane ratio at SGP is 0.97, corroborating that air masses in this area are highly impacted by oil and gas sources. LEF and KEY are two other stations where the model predicts that oil and gas activities make a large contribution to atmospheric abundances of C₂–C₅ alkanes (~25% for C₂H₆ and C₃H₈). The relatively high oil and gas contributions are consistent with Helmig et al. (2016); their analysis shows higher rates of changes between 2009 and 2014 in C₂H₆ and C₃H₈ occurring in sites downwind the central and eastern United States. We note that only a few of long-term stations are ideally located to capture changes related to the major oil and gas source regions that have the highest emissions in the updated 2011NEI. Long-term monitoring stations located in northeastern Colorado, Wyoming, and North Dakota should be considered in order to capture emission changes in the oil and gas sector.

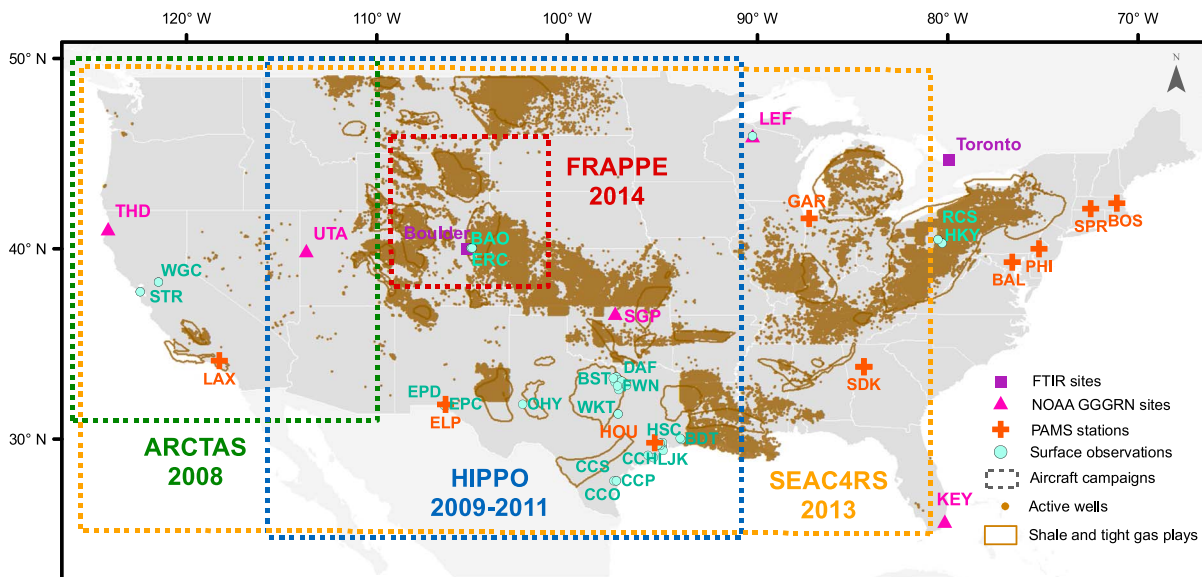


Figure 4. Summary of observations listed in Table 3. Labels of overlapping surface observations are not shown. Locations of active wells come from FracTracker (accessed Nov 2015, www.fractracker.org). In order to provide a sense for well spatial distribution over states with missing data, shale and tight gas plays (Energy Information Administration, accessed Dec 2014, www.eia.gov/dnav/ng/ng_sum_lsum_a_EPG0_xdg_count_a.htm) are shown. FTIR = Fourier transform infrared; NOAA = National Oceanic and Atmospheric Administration; GGGRN = Global Greenhouse Gas Reference Network.

For C_4 - C_5 alkanes, the model shows a stronger seasonality compared to observations and overestimates monthly mean mixing ratios at all the selected stations. The stronger seasonality in the model output compared to observations could be a function of either an incorrect representation of the seasonality of C_4 - C_5 alkane emissions in the updated 2011NEI and/or the use of a single reaction rate for C_4 - C_5 alkanes. Absolute differences between observed and modeled C_4 - C_5 alkane surface mixing ratios are highest at SGP and LEF stations, where the monthly overestimations are as high as 22 ppb C (bottom row of Figure 6). At the THD and UTA stations, the absolute overestimation is not nearly as dramatic as for the other stations; the average annual overestimation for both sites is ~ 1.2 ppbC. However, on an annual

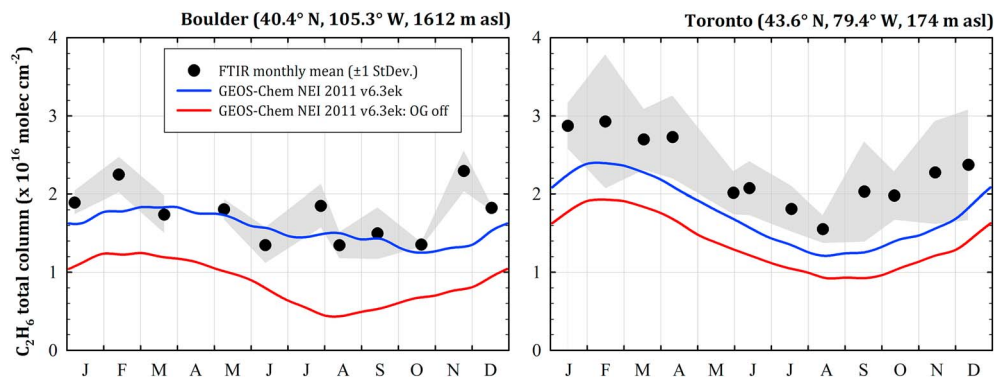


Figure 5. Comparison of 2011 FTIR C_2H_6 total columns to GEOS-Chem C_2H_6 columns using a simulation with and without oil and gas sources from the updated 2011NEI. Black dots represent FTIR monthly mean C_2H_6 total columns, and the gray shading denotes their associated 1σ standard deviation. Monthly means are displayed proportionally to the observations available in each month. The blue line represents modeled C_2H_6 total columns using all sectors from the updated 2011NEI. The red line represents modeled C_2H_6 total columns with C_2H_6 emissions from oil and gas sector turned off (updated 2011NEI: OG off). The blue and red lines are running mean fits to the daily averaged model columns (with a 6-week-wide integration time and a 15-day time step). FTIR = Fourier transform infrared; GEOS = Goddard Earth Observing System; NEI = National Emission Inventory.

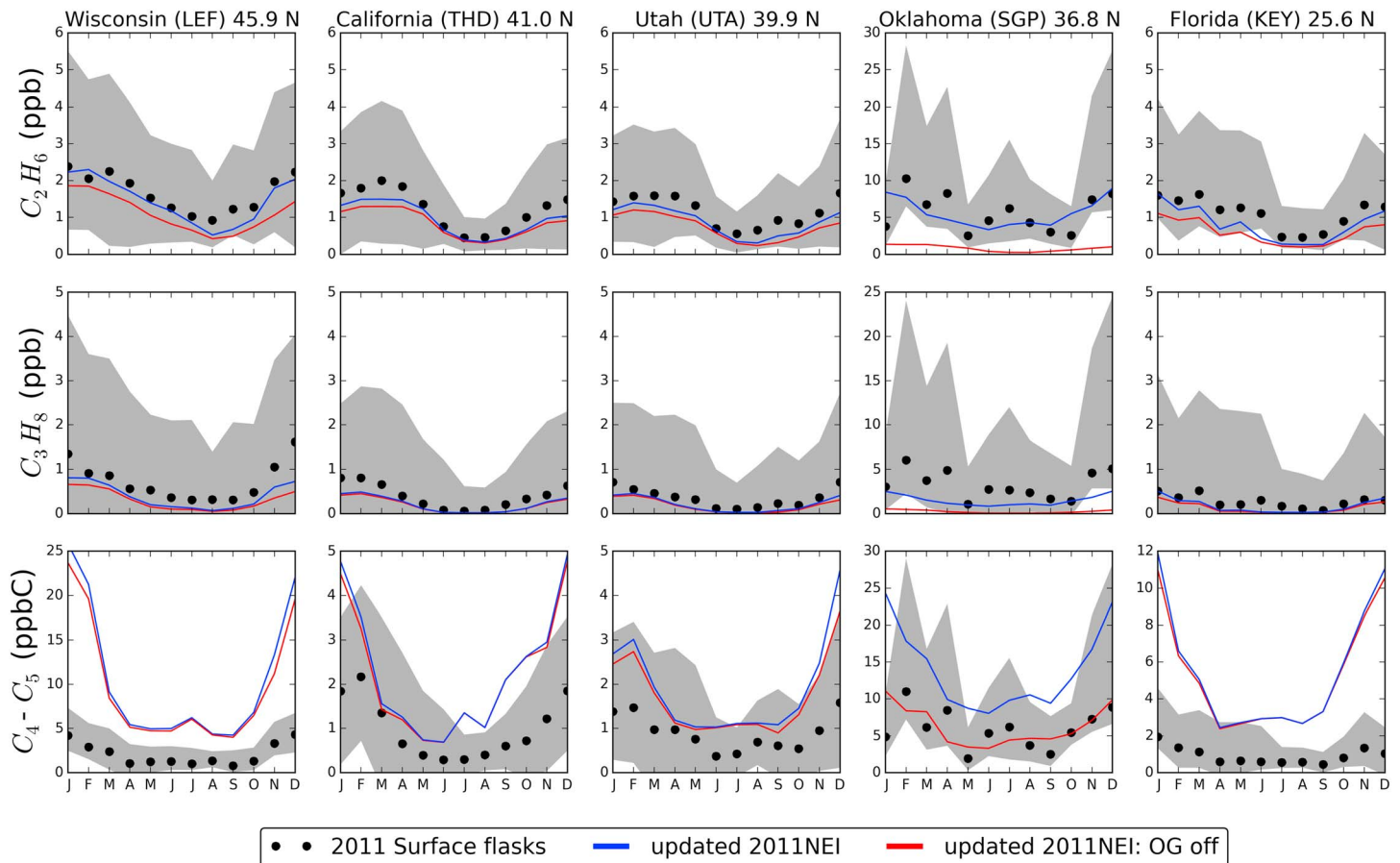


Figure 6. Comparison of 2011 surface mixing ratios for C_2H_6 , C_3H_8 , and C_4-C_5 alkanes (from top to bottom) to modeled 2011 emissions from the updated 2011NEI with and without oil and gas sources. Black dots represent monthly mean observations from National Oceanic and Atmospheric Administration Global Greenhouse Gas Reference Network global surface flask network (Table 3), and the gray areas denote their associated 90th percentile. The blue line represents monthly mean simulated surface mixing ratios using emissions from all sectors of the updated 2011NEI. The red line represents mixing ratios from the updated 2011NEI: OG off simulation. The stations are ordered from higher (left) to lower (right) latitudes. Note the various vertical scales.

average, the model overestimates C_4-C_5 alkanes at all sites by a factor of ~ 4 . The consistent model bias of C_4-C_5 alkane surface mixing ratios suggests that our choice of assigning C_4-C_5 alkanes as a continuous fraction of total PAR emitted species across the CONUS (see section 2.2) should be revisited. Another possible cause is the overestimation of total PAR emissions in the United States.

3.3.3. Seasonal Comparison to Averaged Observational Data Sets

GEOS-Chem averaged seasonal model output for the year 2011 and observed abundances of C_2H_6 , C_3H_8 , and C_4-C_5 alkanes are shown in Figures 7–9, respectively. The bottom row in the upper panels of Figures 7–9 show filled circles that represent seasonal averages of daily surface flask measurements and other surface observations as averages of their specific sampling period in the corresponding season when they occurred. Time periods and locations for each data set are presented in Table 3. As can be noted in Table 3, there are very few aircraft observations for 2011. The upper panels of Figures 7–9 present aircraft observations from other years. Given high rates of change in C_2H_6 and C_3H_8 since 2009, particularly over the central United States (Franco et al., 2016; Helmig et al., 2016), directly comparing the model to these observations is a challenge. We use the observations and model to show seasonal, horizontal, and vertical gradients in these species across the United States. We provide comparisons where we can do so conservatively. In order to provide a direct comparison to surface observations, the lower panels of Figures 7–9 show modeled versus surface flask observations from the year-round TCEQ and INSTARR data sets.

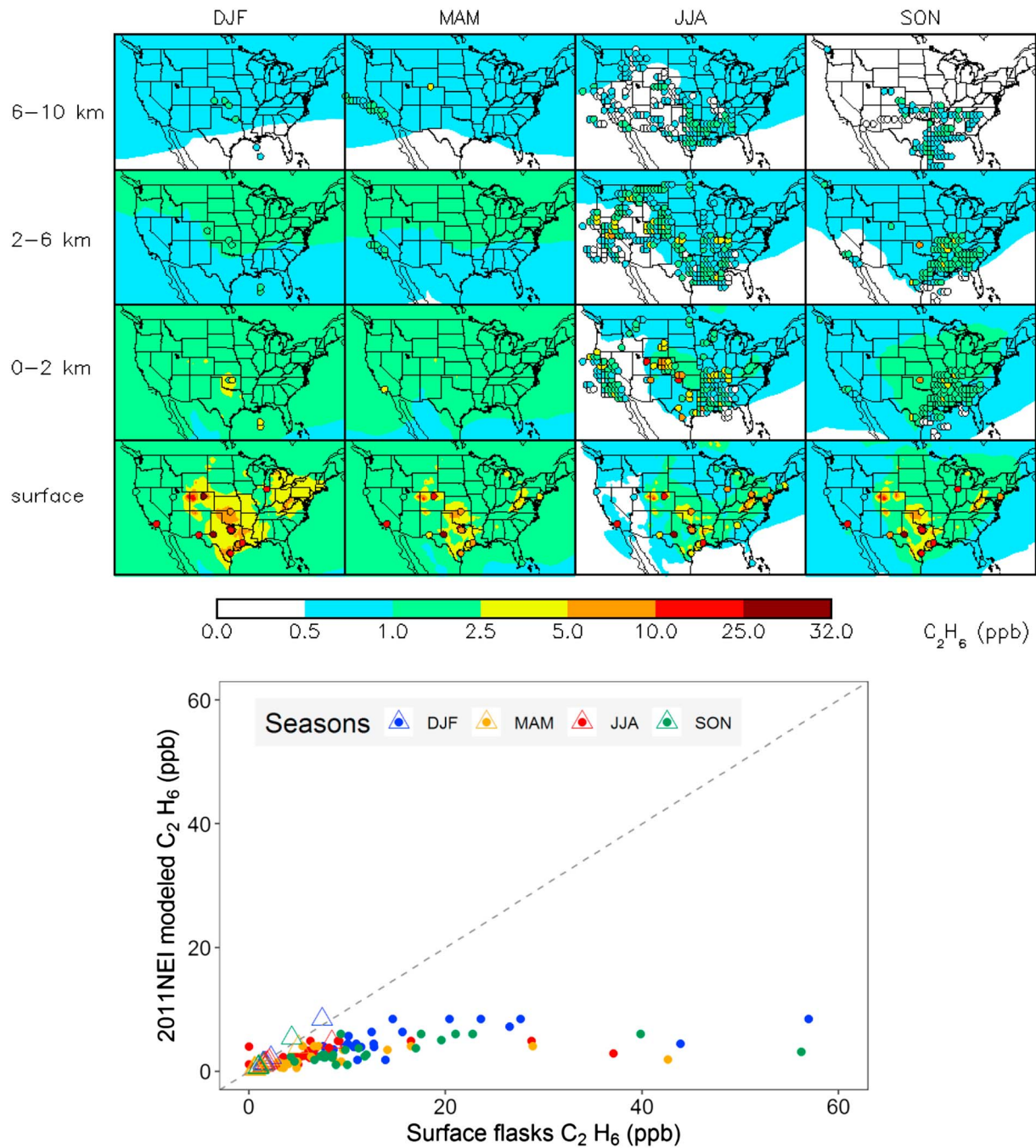


Figure 7. (upper panel) Mean distribution of C_2H_6 abundances for different seasons and altitude ranges compared to observations from aircraft campaigns and surface measurements (Table 3). The background contours are model outputs for 2011. The filled circles represent seasonally averaged observations. Aircraft measurements (0–2, 2–6, and 6–10 km) are averaged vertically for each altitude range and horizontally every $1^\circ \times 1^\circ$. (lower panel) Scatter plot of seasonal surface observations from TCEQ (filled circles) and INSTARR (transparent triangles) data sets. DJF = December–February; MAM = March–May; JJA = June–August; SON = September–November.

Across the United States, there is a seasonal gradient in C_2 – C_5 alkane mixing ratios due to the seasonal variations in OH concentrations (upper panels of Figures 7–9); there are higher C_2 – C_5 alkane mixing ratios during fall and winter compared to spring and summer (more on this in section 3.3.2). Most of the aircraft observations (0–10 km) presented here were collected during summer months. In this season, the

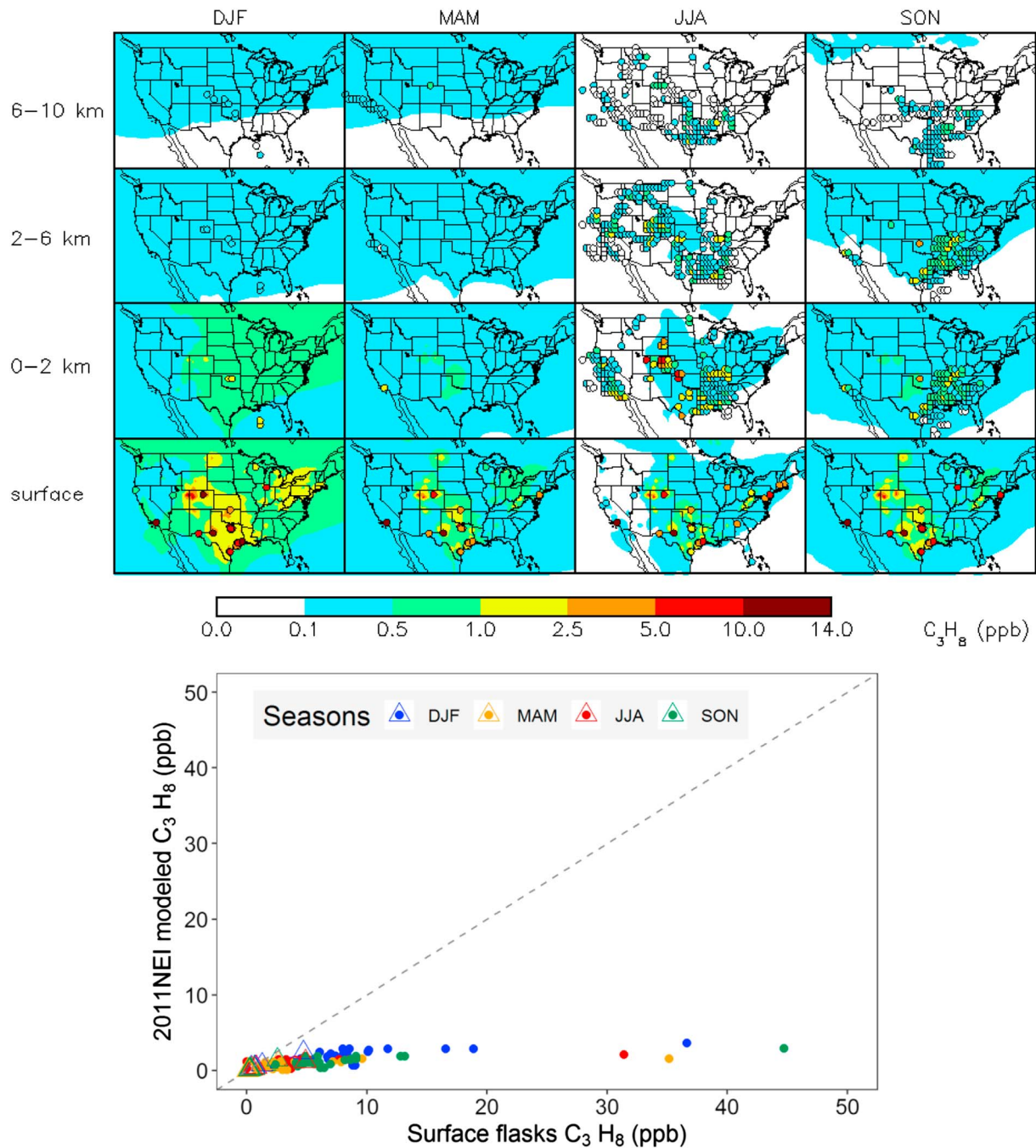


Figure 8. (upper panel) Mean distribution of C_3H_8 abundances for different seasons and altitude ranges compared to observations from aircraft campaigns and surface measurements (Table 3). The background color contours are model outputs for 2011. The filled circles represent seasonally averaged observations. Aircraft measurements (0–2, 2–6, and 6–10 km) are averaged vertically for each altitude range and horizontally every $1^\circ \times 1^\circ$. (lower panel) Scatter plot of seasonal surface observations from TCEQ (filled circles) and INSTARR (transparent triangles) data sets. DJF = December–February; MAM = March–May; JJA = June–August; SON = September–November.

observations cover most of the CONUS. Although the aircraft campaigns occurred during different years (2008–2014), the almost full coverage of the CONUS provides an overview of the spatial distribution of C_2H_6 , C_3H_8 , and C_4 – C_5 mixing ratios. C_2 – C_5 alkane abundances are more homogenous above 2 km compared to the boundary layer. From 2 to 10 km, mixing ratios primarily reflect Northern Hemisphere background abundances, while in the boundary layer enhancements mirror the spatial distribution of

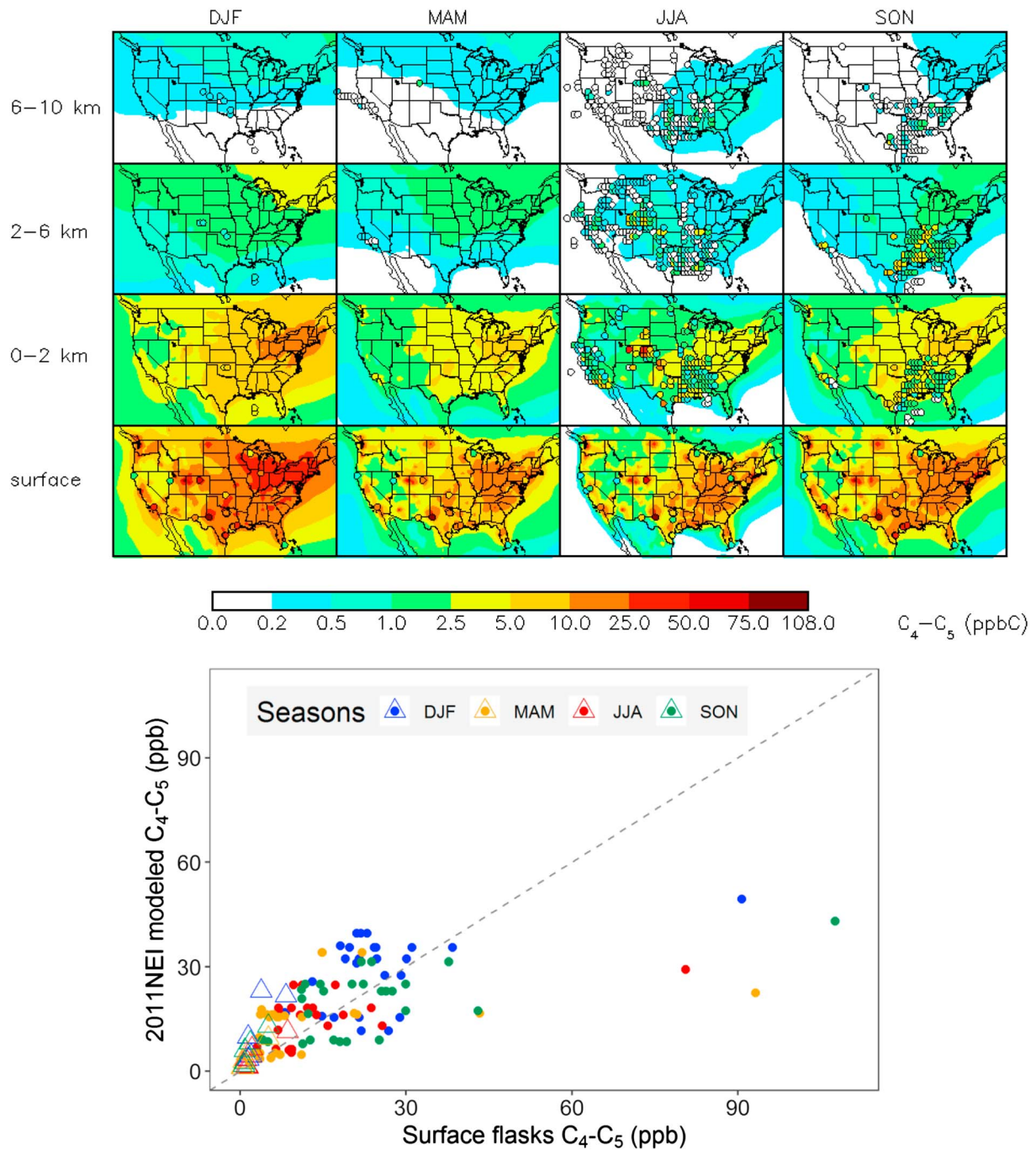


Figure 9. (upper panel) Mean distribution of C_4-C_5 alkane abundances for different seasons and altitude ranges compared to observations from aircraft campaigns and surface measurements (Table 3). The background contours are model outputs for 2011. The filled circles represent seasonally averaged observations. Aircraft measurements (0–2, 2–6, and 6–10 km) are averaged vertically for each altitude range and horizontally every $1^\circ \times 1^\circ$. (lower panel) Scatter plot of seasonal surface observations from TCEQ (filled circles) and INSTARR (transparent triangles) data sets. DJF = December–February; MAM = March–May; JJA = June–August; SON = September–November.

emissions. The largest boundary layer enhancements for these species occur over Colorado, Texas, and Oklahoma. The model output shown in Figures 7–9 corresponds to seasonal averages of monthly means. The spatial distribution of tropospheric abundances is determined by the atmospheric lifetime of each C_2-C_5 alkane. Consequently in our model simulations, tropospheric abundances of C_2H_6 and C_3H_8 are more homogeneous across the CONUS compared to abundances of C_4-C_5 , which show stronger local enhancements below 2 km.

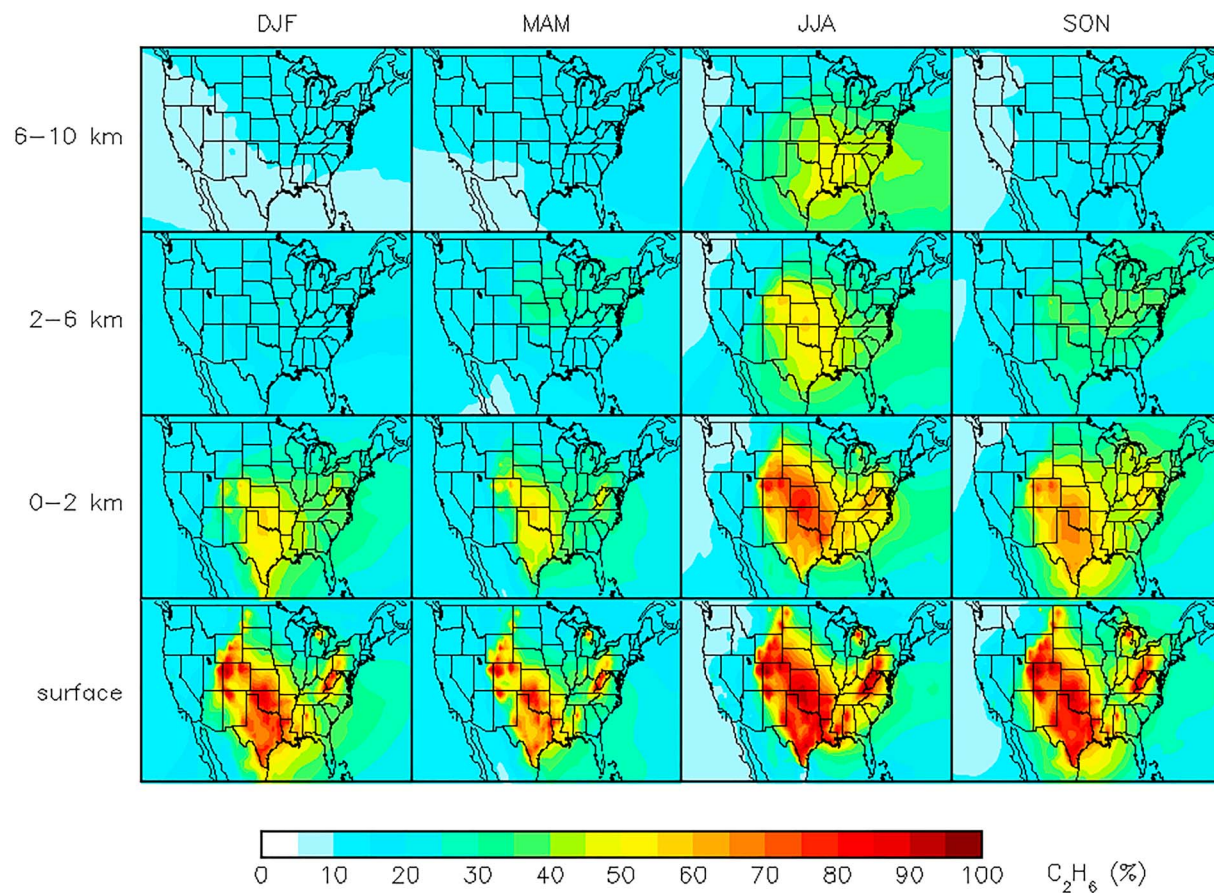


Figure 10. The 2011 simulated percentage contribution from the U.S. oil and gas sector to total abundances of C_2H_6 . DJF = December–February; MAM = March–May; JJA = June–August; SON = September–November.

In some regions (e.g., the Colorado Front Range), most of the observed abundances of C_4 – C_5 alkanes have been attributed to oil and gas activities (Abeleira et al., 2017; Gilman et al., 2013). This is often diagnosed using the ratio of the isomers of butane and pentane (Pétron et al., 2014; Thompson et al., 2014). Enhanced abundances of the C_4 – C_5 alkanes compared to background values are well documented over oil and gas regions (Abeleira et al., 2017; Johansson et al., 2014; Swarthout et al., 2013). For example in the Colorado Front Range, ratios of n-butane, i-pentane, and n-pentane to C_3H_8 in air masses impacted by oil and gas emissions have ranges of 0.43–0.56, 0.13–0.16, and 0.13–0.19, respectively (Gilman et al., 2013; Pétron et al., 2014; Swarthout et al., 2013). In addition to oil and gas sources, typical urban sources of C_4 – C_5 alkanes are landfills (U.S. EPA, 2009) and traffic (Abeleira et al., 2017; Kirchstetter et al., 1996).

A portion of the HIPPO flights did occur in 2011, but only two HIPPO flights (9 and 11 August 2011) cross our region of interest during this period. These two HIPPO flights allow us to make a direct comparison between aircraft observations and model output. We sampled the model at the coincident time and location of the observations from the HIPPO flights on 9 and 11 August 2011. Model bias is largest for C_3H_8 and is only apparent at altitudes below 700 hPa. The normalized mean model bias for C_3H_8 (NMB = sum (model – obs)/(sum (obs))) is –44% for the 9 August 2011 flight and –33% for the 11 August 2011 flight. This supports the conclusion drawn from the surface observation comparison for 2011 (Figure 8 lowest row) that the model underpredicts C_3H_8 mixing ratios.

The SEAC⁴RS observations cover a region of the United States where we would expect a large influence from emissions from the oil and gas sector. The lower panels of Figures 7 and 8 show that the model simulation underpredicts average TCEQ observations of C_2H_6 and C_3H_8 over Texas (filled circles) by ~50% throughout the year. It is likely that there were changes in the average abundance of C_2 – C_5 in this region, even over the 2-year period between 2011 (model output) and 2013 (SEAC⁴RS observations).

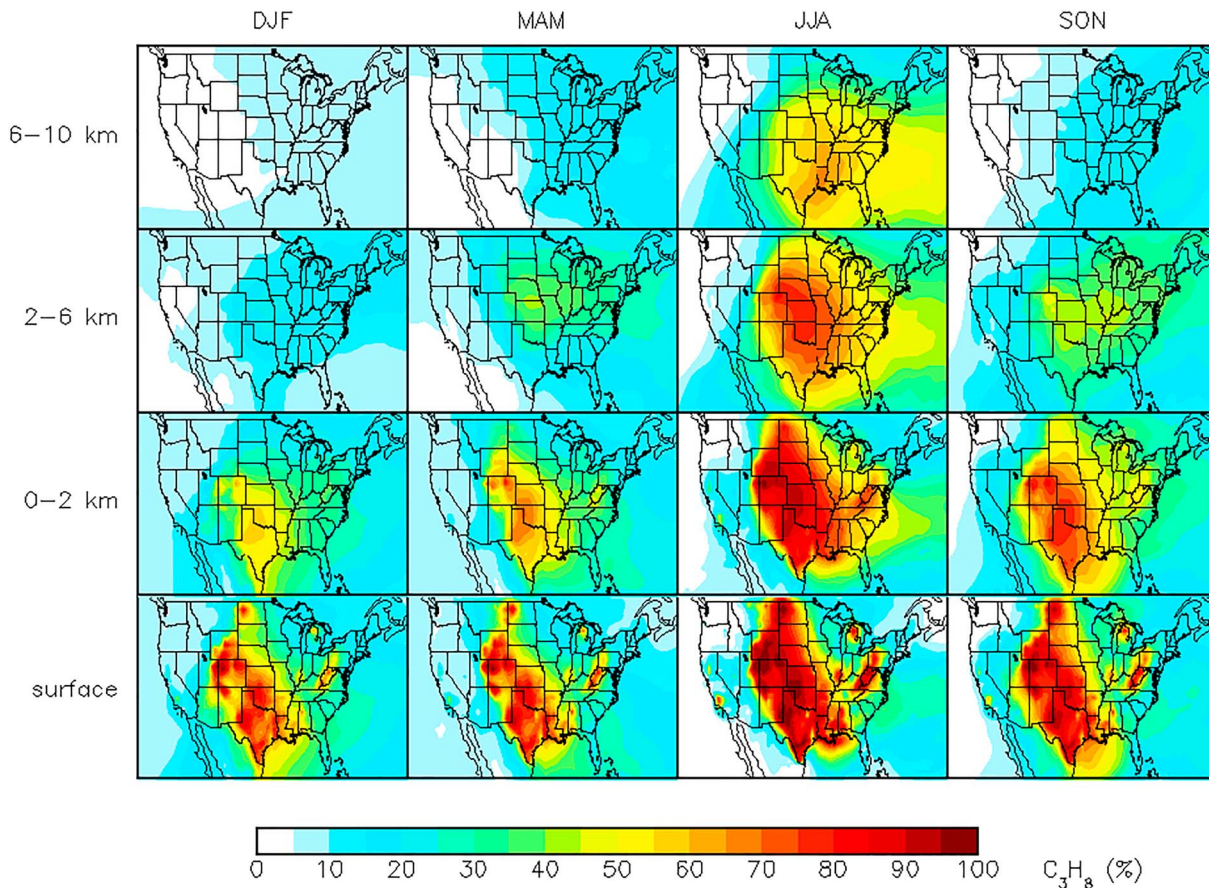


Figure 11. The 2011 simulated percentage contribution from the U.S. oil and gas sector to total abundances of C_3H_8 . DJF = December–February; MAM = March–May; JJA = June–August; SON = September–November.

Helmig et al. (2016) summarize observed trends in C_2H_6 and C_3H_8 over the period 2009–2014 for long-term surface sites. The largest trend in C_3H_8 over the period 2009–2014 in this region in Helmig et al. (2016) is for Moody, Texas. The change is 286 pptv/year. The model, based on 2011 emissions and meteorology, underpredicts the observed 2013 SEAC⁴RS C_3H_8 mixing ratios over Texas below 2 km by ~1 ppbv. Even a trend of 286 pptv/year applied to the SEAC⁴RS data is unlikely to close the model-measurement gap. When we compare average model output to the SEAC⁴RS observations, hypothetical detrending would still result in an underprediction of the observations by >400 pptv. This rough calculation also supports the conclusion that C_3H_8 is underpredicted by the model.

As discussed in section 2.2, the mass-weighted OH concentration for our model simulation is at the upper end of what is reported in other modeling studies. If the OH in the model were higher, this would cause the model lifetime of propane to be shorter than reality and this would cause simulated propane to decay more quickly downwind of sources. However, it seems highly unlikely that our hypothesis that propane emissions are too low is a product of unreasonably high OH concentrations for these reasons. (1) The model bias in propane is only below 700 hPa over the United States when compared to the HIPPO flights. A problem with OH should produce bias outside of the boundary layer over the United States. (2) The model underprediction of the propane at the surface is very large (as shown in Figure 8). In many locations, the model underpredicts propane by almost an order of magnitude. There is no indication that OH is incorrect by an order of magnitude. (3) The model is missing an additional sink of propane (halogens). Adding an additional sink would only serve to push the simulated propane down. This would further support the hypothesis that emissions are too low for this species.

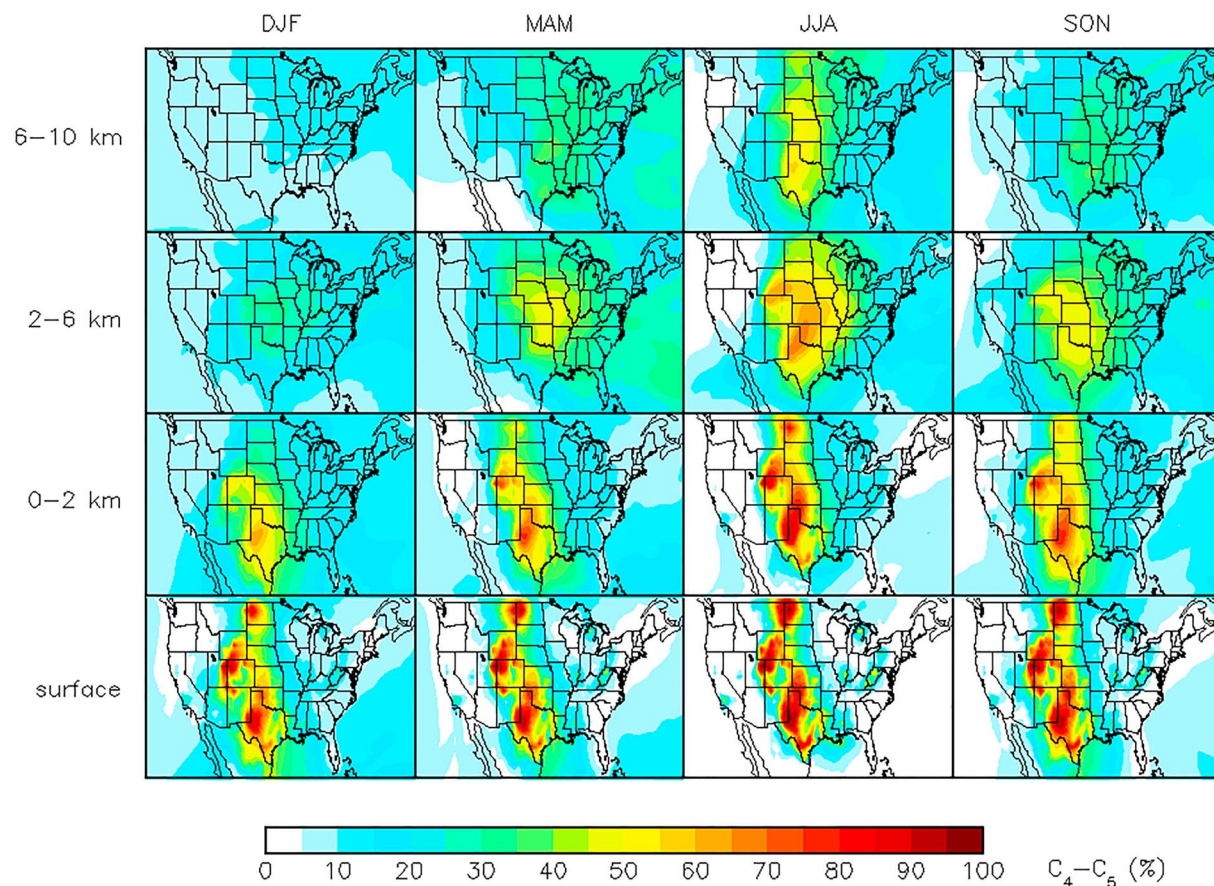


Figure 12. The 2011 simulated percentage contribution from the U.S. oil and gas sector to total abundances of C_4 - C_5 alkanes. DJF = December–February; MAM = March–May; JJA = June–August; SON = September–November.

There is a strong diurnal cycle in the mixing ratios of alkanes within the boundary layer (Abeleira et al., 2017; Vinciguerra et al., 2015). The model output in the upper panels of Figures 7–9 represents seasonal means; thus, the model represents an average of the entire diurnal cycle over these seasons. In contrast, the majority of the aircraft observations were collected during the day when local emissions are mixed into a larger volume and reacting with OH. Despite this, the simulated abundances of C_2H_6 and C_3H_8 at altitudes below 2 km are on average 5 and 3 ppb lower, respectively (both modeled and observed abundances are horizontally averaged every $1^\circ \times 1^\circ$). The discrepancy between the model and the observations is largest for the FRAPPÉ aircraft campaign, which is also the most recent field campaign presented in this study (2014) and encompasses the region with higher annual rates of change of C_2H_6 total column from 2009 to 2014 as estimated by Franco et al. (2016).

Figures 10–12 present the simulated percentage contribution from the oil and gas sector to total abundances of C_2 - C_5 alkanes. We use the updated 2011NEI: OG off simulation to estimate the percentage contribution of emissions from this sector to total C_2 - C_5 alkane mixing ratios. Of the regions examined here, the lowest contribution of U.S. oil and gas activity to surface mixing ratios of C_2 - C_5 alkanes is over California, which has relatively little local oil and gas development compared to the other regions of the United States. Gentner et al. (2009) reported i-pentane/n-pentane ratios for California during summertime ranging from 2.9 for liquid gasoline to 3.8 for gasoline vapors. The June–July mean i-pentane/n-pentane ratios over this area for the 2008 ARCTAS aircraft campaign and 2011 surface flask observations at the LAX station were 2.0 and 2.2, respectively, suggesting that air masses are dominated by urban sources (Figure 11).

Over the central and southeastern United States the model attributes a higher percentage of the near-surface C_2H_6 and C_3H_8 to oil- and gas-related activities, compared to C_4 - C_5 alkanes. Figure 11 shows that the model attributes most of the C_3H_8 at the surface to emissions from the oil and gas sector. The estimated oil and gas

contribution to near-surface C_2H_6 and C_3H_8 mixing ratios over Colorado is consistent with results from Gilman et al. (2013), who estimated mean percentage contributions of 72% and 90%, respectively. However, our estimated contribution from oil and gas sources to C_4 - C_5 alkanes is ~10% lower compared to the Gilman et al. (2013) calculation of 93–96%. This difference suggests that our choice to assign C_4 - C_5 alkanes as 36% of the total emitted PAR species over the United States for all emissions sources should be revisited over regions where oil and gas activities abut urban areas, like Colorado. For the Colorado Front Range, the percentage of C_4 - C_5 alkanes to total emitted PAR species is likely higher than 36%.

Figures 10–12 suggest that emissions over oil and gas regions can impact atmospheric abundances over much of the U.S. lower-to-middle free troposphere. This does not imply that the atmosphere is well mixed over a given area from the surface to 10 km on a given day. Rather, it reflects typical characteristic time scales for vertical transport which are ~1 week for mixing in the lower free troposphere and ~1 month for mixing throughout the troposphere. The lifetimes of C_2H_6 and C_3H_8 are on average sufficiently long such that these species can be mixed vertically. However, we note that alkane lifetimes due to OH reactions can have significant seasonality (Miller et al., 2012). Figures 10 and 11 reflect more vigorous mixing in summer months.

4. Conclusions

We use a GEOS-Chem nested simulation driven by updated 2011NEI emissions in combination with a collection of observations over the United States to (1) examine the spatial patterns in observed atmospheric abundances of C_2 - C_5 alkanes and (2) estimate the contribution of the U.S. oil and gas industry to the observed patterns.

The updated 2011NEI, indicates that the oil and gas sector dominated U.S. emissions of C_2H_6 and C_3H_8 with a contribution to total emissions of 89% and 82%, respectively (U.S. EPA, 2017). Emissions of these two species are largely located inside U.S. oil and gas basins. As implemented in GEOS-Chem, oil and gas sources represent the third most important emission source for C_4 - C_5 alkanes. Other fossil fuel sources contribute significantly to the emissions of these larger alkanes; thus, their emissions are located not only inside oil-and-gas-producing basins but also within urban and industrial areas.

Aircraft observations over the period 2008–2014 show that the highest mixing ratios of C_2 - C_5 alkanes were encountered over the central U.S. boundary layer (mainly over Colorado, Texas, and Oklahoma) during this period. Observations were much more homogenous above 2 km for all the species considered here. Both, the suite of observations and modeled C_2 - C_5 alkane abundances, show that U.S. oil and gas emissions impact large regions of the lower troposphere especially over the central and eastern United States. The surface and limited aircraft observation-model comparisons for C_3H_8 suggest that the emissions of C_3H_8 in the updated 2011NEI may continue to be too low.

Given that increases in C_2 - C_5 alkane abundances driven by emissions from the U.S. oil and gas industry began in 2009, we do not recommend using the updated 2011NEI for prior years. There are many locations where oil and gas development is relatively recent. Similarly, the updated 2011NEI precedes much of the extraction of oil and gas in the Bakken. Thus, if simple scaling factors were to be applied to this inventory for simulations after 2011, we would not expect that the resulting emissions would represent this area well. Furthermore, the reported increasing trends in atmospheric concentrations of oil- and natural gas-related emissions during 2010–2015 (Franco et al., 2016; Helmig et al., 2016; Vinciguerra et al., 2015) suggest that the C_2 - C_5 alkane emission estimates in this paper are likely a low estimate for years following 2011.

Due to the increasing importance of oil and gas emissions in the United States, long-term measurements of C_2 - C_5 alkanes are needed in order to document how the emissions of these species are changing. We recommend continued support of existing long-term measurements of C_2 - C_5 alkanes. We also suggest continuous consistent monitoring of surface mixing ratios in northeastern Colorado, Wyoming, and North Dakota. Further, we suggest that the community evaluate whether chemical mechanisms that lump larger alkanes are sufficient to understand air quality issues in regions with large emissions of these species.

Acknowledgments

Funding for Zitley A. Tzompa-Sosa was provided by Consejo Nacional de Ciencia y Tecnología (CONACYT) under fellowship 216028 and NOAA under award NA14OAR4310148. Support for Emily V. Fischer was provided by the NOAA under award NA14OAR4310148. Emmanuel Mahieu is a Research Associate with the F.R.S.-FNRS. The authors thank the NDACC for FTIR solar data provision. The FTIR data used in this publication are publicly available (see <http://www.ndacc.org>). The Toronto measurements were made at the University of Toronto Atmospheric Observatory (TAO), which has been supported by CFCAS, ABB Bomem, CFI, CSA, ECCS, NSERC, ORDCF, PREA, and the University of Toronto. Analysis of the Toronto NDACC data was supported by the CAFTON project, funded by the Canadian Space Agency's FAST Program. The National Center for Atmospheric Research is sponsored by the National Science Foundation. The NCAR FTIR program is supported under contract by the National Aeronautics and Space Administration (NASA). The VOC analyses by INSTAAR are conducted in samples collected within the NOAA Global Greenhouse Gas Reference Network, which is supported by the NOAA Climate Program Office AC4 Program (data sets are publicly available at <https://www.esrl.noaa.gov/gmd/dv/data/>). The research described in this article has been reviewed by the U.S. Environmental Protection Agency and approved for publication. Approval does not signify that the contents necessarily reflect the views and the policies of the agency nor does mention of trade names or commercial products constitute endorsement or recommendation for use. The updated 2011NEI emission inventory can be accessed via the Colorado State University Digital Repository at <https://hdl.handle.net/10217/187477>.

References

- Abeira, A., Pollack, I. B., Sive, B., Zhou, Y., Fischer, E. V., & Farmer, D. K. (2017). Source characterization of volatile organic compounds in the Colorado Northern Front Range Metropolitan Area during spring and summer 2015. *Journal of Geophysical Research: Atmospheres*, *122*, 3595–3613. <https://doi.org/10.1002/2016jd026227>
- Aceves, M., & Grimalt, J. O. (1993). Seasonally dependent size distributions of aliphatic and polycyclic aromatic hydrocarbons in urban aerosols from densely populated areas. *Environmental Science & Technology*, *27*(13), 2896–2908. <https://doi.org/10.1021/es00049a033>
- Atkinson, R., Baulch, D. L., Cox, R. A., Crowley, J. N., Hampson, R. F., Hynes, R. G., et al. (2006). Evaluated kinetic and photochemical data for atmospheric chemistry: Volume II—Gas phase reactions of organic species. *Atmospheric Chemistry and Physics*, *6*(11), 3625–4055. <https://doi.org/10.5194/acp-6-3625-2006>
- Basevich, V. Y., Belyaev, A. A., Medvedev, S. N., Posvyanskii, V. S., & Frolov, S. M. (2012). Oxidation and combustion mechanisms of paraffin hydrocarbons: Transfer from C₁–C₇ to C₈H₁₈, C₉H₂₀, and C₁₀H₂₂. *Russian Journal of Physical Chemistry B*, *5*(6), 974–990. <https://doi.org/10.1134/s1990793111060194>
- Bey, I., Jacob, D. J., Yantosca, R. M., Logan, J. A., Field, B. D., Fiore, A. M., et al. (2001). Global modeling of tropospheric chemistry with assimilated meteorology: Model description and evaluation. *Journal of Geophysical Research*, *106*(D19), 23,073–23,095. <https://doi.org/10.1029/2001JD000807>
- Bi, X., Sheng, G., Peng, P. a., Chen, Y., & Fu, J. (2005). Size distribution of n-alkanes and polycyclic aromatic hydrocarbons (PAHs) in urban and rural atmospheres of Guangzhou, China. *Atmospheric Environment*, *39*(3), 477–487. <https://doi.org/10.1016/j.atmosenv.2004.09.052>
- Blake, N. J., Barletta, B., Simpson, I. J., Schroeder, J., Hughes, S., Marrero, J. E., et al. (2014). Spatial distributions and source characterization of trace organic gases during SEAC⁴RS and comparison to DC3. paper presented at American Geophysical Union, San Francisco.
- Brandt, A. R., Heath, G. A., & Cooley, D. (2016). Methane leaks from natural gas systems follow extreme distributions. *Environmental Science & Technology*, *50*(22), 12,512–12,520. <https://doi.org/10.1021/es6b04303>
- Brandt, A. R., Heath, G. A., Kort, E. A., O'Sullivan, F., Petron, G., Jordaan, S. M., et al. (2014). Methane leaks from North American natural gas systems. *Science*, *343*(6172), 733–735. <https://doi.org/10.1126/science.1247045>
- Brantley, H. L., Thoma, E. D., & Eisele, A. P. (2015). Assessment of volatile organic compound and hazardous air pollutant emissions from oil and natural gas well pads using mobile remote and on-site direct measurements. *Journal of the Air & Waste Management Association*, *65*(9), 1072–1082. <https://doi.org/10.1080/10962247.2015.1056888>
- Brantley, H. L., Thoma, E. D., Squier, W. C., Guven, B. B., & Lyon, D. (2014). Assessment of methane emissions from oil and gas production pads using mobile measurements. *Environmental Science & Technology*, *48*(24), 14,508–14,515. <https://doi.org/10.1021/es503070q>
- de Gouw, J. A., Parrish, D. D., Frost, G. J., & Trainer, M. (2014). Reduced emissions of CO₂, NO_x, and SO₂ from U.S. power plants owing to switch from coal to natural gas with combined cycle technology. *Earth's Future*, *2*(2), 75–82. <https://doi.org/10.1002/2013ef000196>
- Field, R. A., Soltis, J., McCarthy, M. C., Murphy, S., & Montague, D. C. (2015). Influence of oil and gas field operations on spatial and temporal distributions of atmospheric non-methane hydrocarbons and their effect on ozone formation in winter. *Atmospheric Chemistry and Physics*, *15*(6), 3527–3542. <https://doi.org/10.5194/acp-15-3527-2015>
- Franco, B., Bader, W., Toon, G. C., Bray, C., Perrin, A., Fischer, E. V., et al. (2015). Retrieval of ethane from ground-based FTIR solar spectra using improved spectroscopy: Recent burden increase above Jungfraujoch. *Journal of Quantitative Spectroscopy & Radiative Transfer*, *160*, 36–49. <https://doi.org/10.1016/j.jqsrt.2015.03.017>
- Franco, B., Mahieu, E., Emmons, L. K., Tzompa-Sosa, Z. A., Fischer, E. V., Sudo, K., et al. (2016). Evaluating ethane and methane emissions associated with the development of oil and natural gas extraction in North America. *Environmental Research Letters*, *11*(4), 044010. <https://doi.org/10.1088/1748-9326/11/4/044010>
- Gentner, D. R., Harley, R. A., Miller, A. M., & Goldstein, A. H. (2009). Diurnal and seasonal variability of gasoline-related volatile organic compound emissions in Riverside, California. *Environmental Science & Technology*, *43*(12), 4247–4252. <https://doi.org/10.1021/es9006228>
- Gilman, J. B., Lerner, B. M., Kuster, W. C., & de Gouw, J. A. (2013). Source signature of volatile organic compounds from oil and natural gas operations in northeastern Colorado. *Environmental Science & Technology*, *47*(3), 1297–1305. <https://doi.org/10.1021/es304119a>
- Goetz, J. D., Avery, A., Werden, B., Floerchinger, C., Fortner, E. C., Wormhoudt, J., et al. (2017). Analysis of local-scale background concentrations of methane and other gas-phase species in the Marcellus shale. *Elementa: Science of the Anthropocene*, *5*, 1. <https://doi.org/10.1525/elementa.182>
- Gomer, R., & Kistiakowsky, G. B. (1951). The rate constant of ethane formation from methyl radicals. *The Journal of Chemical Physics*, *19*(1), 85–91. <https://doi.org/10.1063/1.1747995>
- Guo, H. (2012). Volatile organic compounds (VOCs) emitted from petroleum and their influence on photochemical smog formation in the atmosphere. *Journal of Petroleum & Environmental Biotechnology*, *03*(01). <https://doi.org/10.4172/2157-7463.1000e104>
- Halliday, H. S., Thompson, A. M., Wisthaler, A., Blake, D. R., Hornbrook, R. S., Mikoviny, T., et al. (2016). Atmospheric benzene observations from oil and gas production in the Denver-Julesburg Basin in July and August 2014. *Journal of Geophysical Research: Atmospheres*, *121*, 11,055–11,074. <https://doi.org/10.1002/2016JD025327>
- Hannigan, J. W., Coffey, M. T., & Goldman, A. (2009). Semiautonomous FTS observation system for remote sensing of stratospheric and tropospheric gases. *Journal of Atmospheric and Oceanic Technology*, *26*(9), 1814–1828. <https://doi.org/10.1175/2009jtecha1230.1>
- Helmig, D., Rossabi, S., Hueber, J., Tans, P., Montzka, S. A., Masarie, K., et al. (2016). Reversal of global atmospheric ethane and propane trends largely due to US oil and natural gas production. *Nature Geoscience*, *9*(7), 490–495. <https://doi.org/10.1038/ngeo2721>
- Helmig, D., Thompson, C. R., Evans, J., Boylan, P., Hueber, J., & Park, J. H. (2014). Highly elevated atmospheric levels of volatile organic compounds in the Uintah Basin, Utah. *Environmental Science & Technology*, *48*(9), 4707–4715. <https://doi.org/10.1021/es405046r>
- Johansson, J. K. E., Mellqvist, J., Samuelsson, J., Offerle, B., Lefter, B., Rappenglück, B., et al. (2014). Emission measurements of alkenes, alkanes, SO₂, and NO₂ from stationary sources in Southeast Texas over a 5 year period using SOF and mobile DOAS. *Journal of Geophysical Research: Atmospheres*, *119*, 1973–1991. <https://doi.org/10.1002/2013jd020485>
- Kang, M., Kanno, C. M., Reid, M. C., Zhang, X., Mauzerall, D. L., Celia, M. A., et al. (2014). Direct measurements of methane emissions from abandoned oil and gas wells in Pennsylvania. *Proceedings of the National Academy of Sciences of the United States of America*, *111*(51), 18,173–18,177. <https://doi.org/10.1073/pnas.1408315111>
- Keller, C. A., Long, M. S., Yantosca, R. M., Da Silva, A. M., Pawson, S., & Jacob, D. J. (2014). HEMCO v1.0: A versatile, ESMF-compliant component for calculating emissions in atmospheric models. *Geoscientific Model Development*, *7*(4), 1409–1417. <https://doi.org/10.5194/gmd-7-1409-2014>
- Kirchstetter, T. W., Singer, B. C., Harley, R. A., Kendall, G. R., & Chan, W. (1996). Impact of oxygenated gasoline use on California light-duty vehicle emissions. *Environmental Science & Technology*, *30*(2), 661–670. <https://doi.org/10.1021/es950406p>

- Kort, E. A., Smith, M. L., Murray, L. T., Gvakharia, A., Brandt, A. R., Peischl, J., et al. (2016). Fugitive emissions from the Bakken shale illustrate role of shale production in global ethane shift. *Geophysical Research Letters*, *43*, 4617–4623. <https://doi.org/10.1002/2016gl068703>
- Koss, A. R., de Gouw, J., Warneke, C., Gilman, J. B., Lerner, B. M., Graus, M., et al. (2015). Photochemical aging of volatile organic compounds associated with oil and natural gas extraction in the Uintah Basin, UT, during a wintertime ozone formation event. *Atmospheric Chemistry and Physics*, *15*(10), 5727–5741. <https://doi.org/10.5194/acp-15-5727-2015>
- Kuhns, H., Green, M., & Etyemezian, V. (2003). *Big bend regional aerosol and visibility observational (BRAVO) study emissions InventoryRep*. Las Vegas, NV: Desert Research Institute.
- Lee, B. H., Munger, J. W., Wofsy, S. C., & Goldstein, A. H. (2006). Anthropogenic emissions of nonmethane hydrocarbons in the north-eastern United States: Measured seasonal variations from 1992–1996 and 1999–2001. *Journal of Geophysical Research*, *111*, D20307. <https://doi.org/10.1029/2005JD006172>
- Lurmann, F. W., Lloyd, A. C., & Atkinson, R. (1986). A chemical mechanism for use in long-range transport/acid deposition computer modeling. *Journal of Geophysical Research*, *91*(D10), 10,905–10,936. <https://doi.org/10.1029/JD091iD10p10905>
- Miller, J. B., Lehman, S. J., Montzka, S. A., Sweeney, C., Miller, B. R., Karion, A., et al. (2012). Linking emissions of fossil fuel CO₂ and other anthropogenic trace gases using atmospheric ¹⁴C. *Journal of Geophysical Research*, *117*, D08302. <https://doi.org/10.1029/2011JD017048>
- Mitchell, A. L., Tkacik, D. S., Roscioli, J. R., Herndon, S. C., Yacovitch, T. I., Martinez, D. M., et al. (2015). Measurements of methane emissions from natural gas gathering facilities and processing plants: Measurement results. *Environmental Science & Technology*, *49*(5), 3219–3227. <https://doi.org/10.1021/es5052809>
- Naik, V., Voulgarakis, A., Fiore, A. M., Horowitz, L. W., Lamarque, J. F., Lin, M., et al. (2013). Preindustrial to present-day changes in tropospheric hydroxyl radical and methane lifetime from the Atmospheric Chemistry and Climate Model Intercomparison Project (ACCMIP). *Atmospheric Chemistry and Physics*, *13*(10), 5277–5298. <https://doi.org/10.5194/acp-13-5277-2013>
- Pacsi, A. P., Kimura, Y., McGaughey, G., McDonald-Buller, E. C., & Allen, D. T. (2015). Regional ozone impacts of increased natural gas use in the Texas power sector and development in the Eagle Ford shale. *Environmental Science & Technology*, *49*(6), 3966–3973. <https://doi.org/10.1021/es5055012>
- Peischl, J., Karion, A., Sweeney, C., Kort, E. A., Smith, M. L., Brandt, A. R., et al. (2016). Quantifying atmospheric methane emissions from oil and natural gas production in the Bakken shale region of North Dakota. *Journal of Geophysical Research: Atmospheres*, *121*, 6101–6111. <https://doi.org/10.1002/2015JD024631>
- Peischl, J., Ryerson, T. B., Aikin, K. C., de Gouw, J. A., Gilman, J. B., Holloway, J. S., et al. (2015). Quantifying atmospheric methane emissions from the Haynesville, Fayetteville, and northeastern Marcellus shale gas production regions. *Journal of Geophysical Research: Atmospheres*, *120*, 2119–2139. <https://doi.org/10.1002/2014JD022697>
- Pétron, G., Frost, G., Miller, B. R., Hirsch, A. I., Montzka, S. A., Karion, A., et al. (2012). Hydrocarbon emissions characterization in the Colorado Front Range: A pilot study. *Journal of Geophysical Research*, *117*, D04304. <https://doi.org/10.1029/2011JD016360>
- Pétron, G., Karion, A., Sweeney, C., Miller, B. R., Montzka, S. A., Frost, G. J., et al. (2014). A new look at methane and nonmethane hydrocarbon emissions from oil and natural gas operations in the Colorado Denver-Julesburg Basin. *Journal of Geophysical Research: Atmospheres*, *119*, 6836–6852. <https://doi.org/10.1002/2013JD021272>
- Phillips-Smith, C., Jeong, C.-H., Healy, R. M., Dabek-Zlotorzynska, E., Celso, V., Brook, J. R., & Evans, G. (2017). Sources of particulate matter in the Athabasca oil sands region: Investigation through a comparison of trace element measurement methodologies. *Atmospheric Chemistry and Physics Discussions*, *17*(15), 9435–9449. <https://doi.org/10.5194/acp-17-9435-2017>
- Pusede, S. E., & Cohen, R. C. (2012). On the observed response of ozone to NO_x and VOC reactivity reductions in San Joaquin Valley California 1995–present. *Atmospheric Chemistry and Physics*, *12*(18), 8323–8339. <https://doi.org/10.5194/acp-12-8323-2012>
- Rappenglück, B., Ackermann, L., Alvarez, S., Golovko, J., Buhr, M., Fiedl, R. A., et al. (2014). Strong wintertime ozone events in the Upper Green River basin, Wyoming. *Atmospheric Chemistry and Physics*, *14*(10), 4909–4934. <https://doi.org/10.5194/acp-14-4909-2014>
- Richter, D., Weibring, P., Walega, J. G., Fried, A., Spuler, S. M., & Taubman, M. S. (2015). Compact highly sensitive multi-species airborne mid-IR spectrometer. *Applied Physics B*, *119*(1), 119–131. <https://doi.org/10.1007/s00340-015-6038-8>
- Roest, G., & Schade, G. (2017). Quantifying alkane emissions in the Eagle Ford Shale using boundary layer enhancement. *Atmospheric Chemistry and Physics*, *17*(18), 11,163–11,176. <https://doi.org/10.5194/acp-17-11163-2017>
- Roscioli, J. R., Yacovitch, T. I., Floerchinger, C., Mitchell, A. L., Tkacik, D. S., Subramanian, R., et al. (2015). Measurements of methane emissions from natural gas gathering facilities and processing plants: Measurement methods. *Atmospheric Measurement Techniques*, *8*(5), 2017–2035. <https://doi.org/10.5194/amt-8-2017-2015>
- Rossabi, S., & Helmig, D. (2018). Changes in atmospheric butanes and pentanes and their isomeric ratios in the continental United States. *Journal of Geophysical Research: Atmospheres*, *123*, 3772–3790. <https://doi.org/10.1002/2017jd027709>
- Sangwan, M., Yan, C., Chesnokov, E. N., & Krasnoperov, L. N. (2015). Reaction CH₃ + CH₃ → C₂H₆ studied over the 292–714 K temperature and 1–100 bar pressure ranges. *The Journal of Physical Chemistry*, *119*(28), 7847–7857. <https://doi.org/10.1021/acs.jpca.5b01276>
- Schauer, J. J., Kleeman, M. J., Cass, G. R., & Simoneit, B. R. (2002). Measurement of emissions from air pollution sources. 5. C-1–C-32 organic compounds from gasoline-powered motor vehicles. *Environmental Science & Technology*, *36*(6), 1169–1180. <https://doi.org/10.1021/es0108077>
- Schauffler, S., Atlas, E. L., Navarro, M. A., Pan, L., Blake, D. R., Blake, N. J., et al. (2014). *Organic halogen and hydrocarbon distributions during SEAC⁴RS measured from the ER-2 and DC-8*. San Francisco, CA: American Geophysical Union.
- Sherwen, T., Schmidt, J. A., Evans, M. J., Carpenter, L. J., Großmann, K., Eastham, S. D., et al. (2016). Global impacts of tropospheric halogens (Cl, Br, I) on oxidants and composition in GEOS-Chem. *Atmospheric Chemistry and Physics*, *16*(18), 12,239–12,271. <https://doi.org/10.5194/acp-16-12239-2016>
- Simon, H., Beck, L., Bhawe, P. V., Divita, F., Hsu, Y., Luecken, D., et al. (2010). The development and uses of EPA's SPECIATE database. *Atmospheric Pollution Research*, *1*(4), 196–206. <https://doi.org/10.5094/apr.2010.026>
- Simpson, I. J., Akagi, S. K., Barletta, B., Blake, N. J., Choi, Y., Diskin, G. S., et al. (2011). Boreal forest fire emissions in fresh Canadian smoke plumes: C1–C10 volatile organic compounds (VOCs), CO₂, CO, NO₂, NO, HCN and CH₃CN. *Atmospheric Chemistry and Physics*, *11*(13), 6445–6463. <https://doi.org/10.5194/acp-11-6445-2011>
- Simpson, I. J., Blake, N. J., Barletta, B., Diskin, G. S., Fuelberg, H. E., Gorham, K., et al. (2010). Characterization of trace gases measured over Alberta oil sands mining operations: 76 speciated C₂–C₁₀ volatile organic compounds (VOCs), CO₂, CH₄, CO, NO, NO₂, NO_y, O₃ and SO₂. *Atmospheric Chemistry and Physics*, *10*(23), 11,931–11,954. <https://doi.org/10.5194/acp-10-11931-2010>
- Simpson, I. J., Sulbaek Andersen, M. P., Meinardi, S., Bruhwiler, L., Blake, N. J., Helmig, D., et al. (2012). Long-term decline of global atmospheric ethane concentrations and implications for methane. *Nature*, *488*(7412), 490–494. <https://doi.org/10.1038/nature11342>

- Swarthout, R. F., Russo, R. S., Zhou, Y., Hart, A. H., & Sive, B. C. (2013). Volatile organic compound distributions during the NACHTT campaign at the Boulder Atmospheric Observatory: Influence of urban and natural gas sources. *Journal of Geophysical Research: Atmospheres*, *118*, 10,614–10,637. <https://doi.org/10.1002/jgrd.50722>
- Swarthout, R. F., Russo, R. S., Zhou, Y., Miller, B. M., Mitchell, B., Horsman, E., et al. (2015). Impact of Marcellus Shale natural gas development in Southwest Pennsylvania on volatile organic compound emissions and regional air quality. *Environmental Science & Technology*, *49*(5), 3175–3184. <https://doi.org/10.1021/es504315f>
- TCEQ (2012). Texas Commission on Environmental Quality, Texas, USA. Retrieved from <https://www.tceq.texas.gov/>
- Thompson, C. R., Hueber, J., & Helmig, D. (2014). Influence of oil and gas emissions on ambient atmospheric non-methane hydrocarbons in residential areas of northeastern Colorado. *Elementa: Science of the Anthropocene*, *2*, 000035. <https://doi.org/10.12952/journal.elementa.000035>
- Thompson, T. M., Shepherd, D., Stacy, A., Barna, M. G., & Schichtel, B. A. (2017). Modeling to evaluate contribution of oil and gas emissions to air pollution. *Journal of the Air & Waste Management Association*, *67*(4), 445–461. <https://doi.org/10.1080/10962247.2016.1251508>
- Thynne, J. C. J. (1962). Reactions of alkyl radicals. Part 1.—Methyl radical photosensitized decomposition of ethyl formate. *Transactions of the Faraday Society*, *58*(0), 676–684. <https://doi.org/10.1039/tf9625800676>
- Tzompa-Sosa, Z. A., Mahieu, E., Franco, B., Keller, C. A., Turner, A. J., Helmig, D., et al. (2017). Revisiting global fossil fuel and biofuel emissions of ethane. *Journal of Geophysical Research: Atmospheres*, *122*, 2493–2512. <https://doi.org/10.1002/2016JD025767>
- U.S. Energy Information Administration (2017). U.S. Natural gas gross withdrawals and production, Edited by Energy Information Administration.
- U.S. Environmental Protection Agency (2009). Municipal solid waste landfills, edited by A. E. F. a. Quantification.
- U.S. Environmental Protection Agency (2016a). In O. O. A. R. A. O. O. A. Q. P. A. Standards, & U.S. Environmental Protection Agency (Eds.), *Control techniques guidelines for the oil and natural gas industry*. North Carolina, USA: Research Triangle Park.
- U.S. Environmental Protection Agency (2016b). Technical support document: Preparation of emissions inventories for the version 6.3, 2011 emissions modeling platform, Edited by Environmental Protection Agency.
- U.S. Environmental Protection Agency (2017). *National Emissions Inventory 2011, version 6.3ek*. Washington, DC: Environmental Protection Agency.
- Vinciguerra, T., Yao, S., Dadzie, J., Chittams, A., Deskins, T., Ehrman, S., & Dickerson, R. R. (2015). Regional air quality impacts of hydraulic fracturing and shale natural gas activity: Evidence from ambient VOC observations. *Atmospheric Environment*, *110*, 144–150. <https://doi.org/10.1016/j.atmosenv.2015.03.056>
- Voulgarakis, A., Naik, V., Lamarque, J. F., Shindell, D. T., Young, P. J., Prather, M. J., et al. (2013). Analysis of present day and future OH and methane lifetime in the ACCMIP simulations. *Atmospheric Chemistry and Physics*, *13*(5), 2563–2587. <https://doi.org/10.5194/acp-13-2563-2013>
- Warneke, C., Geiger, F., Edwards, P. M., Dube, W., Pétron, G., Kofler, J., et al. (2014). Volatile organic compound emissions from the oil and natural gas industry in the Uintah Basin, Utah: Oil and gas well pad emissions compared to ambient air composition. *Atmospheric Chemistry and Physics*, *14*(20), 10,977–10,988. <https://doi.org/10.5194/acp-14-10977-2014>
- Wiacek, A., Taylor, J. R., Strong, K., Saari, R., Kerzenmacher, T. E., Jones, N. B., & Griffith, D. W. T. (2007). Ground-based solar absorption FTIR spectroscopy: Characterization of retrievals and first results from a novel optical design instrument at a new NDACC Complementary Station. *Journal of Atmospheric and Oceanic Technology*, *24*(3), 432–448. <https://doi.org/10.1175/jtech1962.1>
- Wofsy, S. C., Daube, B., Jimenez, R., Kort, E., Pittman, J. V., Park, S., et al. (2012). HIPPO combined discrete flask and GC sample GHG, halo-, hydrocarbon data (R_20121129), edited by O. R. N. L. Carbon Dioxide Information Analysis Center, Oak Ridge, Tennessee, U.S.A.
- Xiao, Y. P., Logan, J. A., Jacob, D. J., Hudman, R. C., Yantosca, R. M., & Blake, D. R. (2008). Global budget of ethane and regional constraints on US sources. *Journal of Geophysical Research*, *113*, D21306. <https://doi.org/10.1029/2007JD009415>
- Yevich, R., & Logan, J. A. (2003). An assessment of biofuel use and burning of agricultural waste in the developing world. *Global Biogeochemical Cycles*, *17*(4), 1095. <https://doi.org/10.1029/2002GB001952>
- Zielinska, B., Campbell, D., & Samburova, V. (2014). Impact of emissions from natural gas production facilities on ambient air quality in the Barnett Shale area: A pilot study. *Journal of the Air & Waste Management Association*, *64*(12), 1369–1383. <https://doi.org/10.1080/10962247.2014.954735>